Chapter 3

Analytic model of the simulation

This chapter presents analytic models for the bulk and the sheaths, results from which are compared to the PIC simulation. Results from other numerical codes are also compared to the PIC and analytic results. As mentioned in Chapter 1 most of the PIC simulations were run using atomic hydrogen gas with collisional electrons and collisionless ions. These conditions were chosen since cross-sections for hydrogen are well known, and having the lightest ion mass hydrogen reaches steady-state conditions quickly. These simulations were primarily designed to determine the effect of the "external" or applied parameters – such as area ratio, voltage, pressure and frequency (as detailed in Table 2.1) – on the "internal" plasma characteristics, that is the electron temperature, the average potential and density distributions, ion currents, sheath widths etc.

In numerical work the number of diagnostics included is essentially limited only by time constraints for computation – this potentially means there is a vast body of information about the plasma for each different set of conditions. The problem is then to organise this information into some meaningful form, such as scaling laws relating the external input parameters to the internal plasma parameters, in order to further understand the physical processes driving the plasma. Furthermore it is desirable to check the validity of the PIC model, by determining whether the physical picture derived from it accords with other numerical and analytic models. Comparison to experimental results is not really possible for the parameters shown in Table 2.1, since these conditions were not chosen to represent a real physical system, rather they represent a simplified view for comparison with one dimensional models. Hence the analytic model presented here was designed to incorporate the physical features of the PIC code – spherical geometry, collisionless ions - and by tailoring the analytic model to fit the simulation results an understanding of the important physics in the simulation and the consequent effect on the macroscopic behaviour of the plasma is obtained.

Low pressure capacitively coupled rf systems have been quite intensively modelled over the past twenty years or so, because of their technical applications in the materials processing industry. A number of analytic models, including assumptions and

Figure 4.27 shows a phase space plot for the ions, radial position is plotted along the x-axis and velocity along the y-axis, with positive velocity indicating motion to the right and negative motion to the left. This shows clearly the separation between motion in the sheaths and the bulk - considering an ion moving out to the centre of the plasma, it is accelerated slowly until it reaches a critical velocity, whereupon it undergoes rapid acceleration. Due to inertia the ions can only react to the time-averaged fields and so the phase plot delineates the distribution of the average fields in the bulk and the sheath. In order to satisfy Bohm's criterion for the sheath, a region of the bulk with small average fields exists to accelerate ions to velocities greater than or equal to the ion acoustic velocity at the bulk-sheath interface. This region is known as the pre-sheath and in collisional plasmas it is restricted to the region immediately adjacent to the sheath, but in the simulation ions are collisionless and so the pre-sheath fields penetrate through the whole bulk. Once the ions have reached the sheath edge the large fields in the sheath accelerate them toward the electrode. The magnitude of the potential across the sheath can be related to the ion flux at the sheath edge and the sheath width through the sheath equation, which is derived in Section 3.1.

In Section 3.1.1 a dc sheath model is developed, following the technique originally used by Langmuir and Blodgett (1924). In Section 3.1.2 the effect of the rf voltage on the average density in the sheath is examined using results from the simulation, and an equation for the total charge density is developed. In Section 3.1.2 the sheath law for the rf case is derived. In Section 3.2 a model of the plasma bulk is derived from simple kinetic techniques, following the method used by Tonks and Langmuir (1929). The model includes equations for the bulk potential and density distributions, the average electron temperature, the bulk width and the ion currents at the sheath edges. Comparison of bulk parameters to kinetic and fluid models presented by Bissell *et al* (1989) is given in Section 3.2.7. Finally, in Section 3.3 some scaling laws are derived from the simulation, in order to close the set of equations required by the model to fully describe the plasma.

3.1 Spherical sheath law

Langmuir (1924) developed an equation to determine the relationship between the sheath width, the ion current density and the sheath potential for a collisionless dc discharge. This is still used today in the familiar form of the Child-Langmuir sheath equation. Although it was derived for dc conditions, it is also applicable in determining the ion sheath in rf plasmas, since in general the ions cannot respond at rf frequencies due to their inertia and so their behaviour is dependent on the time-averaged or dc

potential across the sheath. Originally derived for a planar electrode system, Langmuir and Blodgett (1924) expanded the derivation to include cylindrical and spherical electrodes. One drawback in using this equation to compare to the simulation is that, since it was derived for a dc system, electrons are completely excluded from the sheath. However, for an rf system the sheath collapses once each rf cycle to allow electrons to escape and balance the ion loss from the system. This has a discernible effect on the average total density in the sheath and consequentially on the sheath potential, although it is often ignored. Lieberman (1988) has calculated the effect of the electron incursion on a planar rf sheath, and found that it modified the sheath law by a constant factor. However, this has not previously been determined for the case of sheaths in a system with spherical electrodes.

The following describes the derivation of an equation for a collisionless sheath using Poisson's equation and current continuity. In section 3.1.1 the dc case is derived obtaining a similar result to that of Langmuir and Blodgett (1924), although the equation is presented in a different form. In section 3.1.2 the change in the average density in an the rf sheath due to the periodic incursion of electrons is determined and in Section 3.1.3 the sheath law is modified for rf conditions.

First of all the sheath equations for the general case are derived. Poisson's equation is used to describe the potential distribution in the sheath

$$\varepsilon_o \nabla^2 \phi(r, t) = -e\,(\overline{n_i - n_e}), \tag{3.1}$$

where ϕ is the time-averaged potential, n_i and n_e are the ion and electron densities in the sheath, and $\overline{n_i - n_e}$ is the time-averaged total charge density. The ion current density at any position is determined by the average ion flux, and hence is a function of the density and the average ion velocity

$$j(r) = e\,n_i(r)\bar{u}(r) = \frac{i}{4\pi r^2}, \tag{3.2}$$

where $\bar{u}$ is the average ion velocity and n_i the ion density at position r. There can be some slight variation of the ion density in the sheath at rf conditions but this is extremely small at applied frequencies of 10 MHz and is neglected here.

In order to simplify calculations in the sheath a new coordinate system in x is introduced which has the origin, $x = 0$, at the position of the sheath edge, r_s, so that the electrode is at position $x=s$, where s is the maximum sheath width. Thus a position x_p in the sheath has a radial distance from the centre equal to $r_p = r_s \pm x_p$, where + is used for the sheath at the outer electrode and - for the inner electrode. The sheath

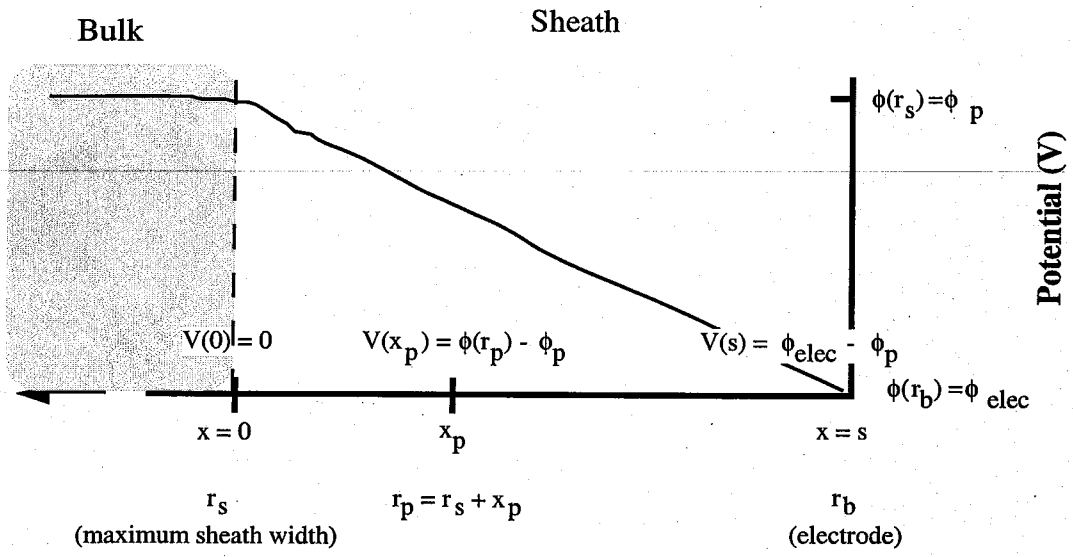

Figure 3.1 Schematic showing coordinate system in x for the sheath (at the outer electrode). The potential in the sheath relative to the bulk potential, V, is shown as a function of x.

potential, V, is measured relative to the plasma potential, ϕ_p, so the sheath potential at x_p is given by $V(x) = \phi_p - \phi(r_p)$, with the boundary conditions are $V(0) = 0$ and $V(s) \equiv V_s = \phi_p - \phi_{elec}$. The new coordinate system is shown schematically in Figure 3.1. Note that in this model the thin sheath approximation is not used, so that sheath calculations are performed in the full spherical coordinate system.

According to the Bohm criterion the ions must enter the sheath with a directed velocity greater than or equal to the ion acoustic velocity, u_B. Assuming that the Bohm criterion is met exactly, and using equation (3.2), then the current at the sheath edge is given by

$$i = 4\pi r_s^2 j_s = 4\pi r_s^2 e n_s u_B, \tag{3.3}$$

where n_s is the ion density at the sheath edge and r_s is the radius of the sheath edge. As ions enter the sheath they are accelerated by the fields. This model assumes collisionless ions, so from conservation of energy the ion velocity at any position x is determined by the potential drop between the sheath edge and x

$$\tfrac{1}{2} m_i \left(u(x)^2 - u_B^2 \right) = -eV(x),$$

$$u(x) = \sqrt{u_B^2 - \frac{2eV(x)}{m_i}}. \tag{3.4}$$

Note that V is negative, since the increase in velocity is due to a drop in the potential. As the ions are accelerated in the sheath fields there is a decrease in density approaching the electrode (this is shown schematically in Figure 3.2). The ion current, however, must be independent of position if there is no ionisation within the sheath since current continuity dictates that the number of ions hitting the electrode must equal the number entering the sheath. For low pressures, that is $p < 100$ mtorr, this is a reasonable assumption since the collision frequency per electron is small and the average electron density in the sheath is also small. Thus by comparing the current at the sheath edge to the current at position x the dependance of the density on position, $n(x)$, can be determined. Equating the current at the sheath edge, equation (3.3), with the current at position x

$$i = 4\pi(r_s + x)^2 e n_i(x)\left(u_B{}^2 - \frac{2eV(x)}{m_i}\right)^{1/2} = 4\pi r_s{}^2 e n_s u_B. \qquad (3.5)$$

Rearranging (3.5) then gives the ion density at any position in the sheath:

$$n_i(x) = \frac{r_s{}^2 n_s u_B}{(r_s + x)^2\sqrt{u_B{}^2 - 2eV(x)/m_i}}$$

$$= \frac{n_s}{\left(1+\frac{x}{r_s}\right)^2\sqrt{1-\frac{2eV(x)}{m_i u_B{}^2}}}. \qquad (3.6)$$

Having determined the ion density in the sheath, it is necessary to find an equation for the electron density in order to obtain the total average charge density to use in Poisson's equation (3.1). This depends on the assumptions used for the sheath physics – the following sections derives equations for the dc and rf sheaths.

3.1.1 Spherical dc sheath equation: $n_e = 0$

For the dc case the sheath width is constant and so electrons are excluded from the sheath region at all times (n.b. this derivation assumes no secondary electrons). Hence the average electron sheath density in equation (3.1) can simply be set to zero, thus making the total charge density equal to the ion density. Substituting equation (3.6) into (3.1) and expanding ∇^2 in terms of one-dimensional spherical coordinates gives an equation for the potential in the sheath of

$$\frac{\partial^2 V}{\partial x^2}+\frac{2}{(r_s+x)}\frac{\partial V}{\partial x}=-\frac{e n_s}{\varepsilon_o\left(1+\frac{x}{r_s}\right)^2\sqrt{1-\frac{2eV(x)}{m_i u_B{}^2}}}. \qquad (3.7)$$

Introducing normalised variables $\eta = 1 - \frac{2eV}{m_i\, u_B{}^2}$ and $z = \frac{x}{r_s}$ to make the calculation simpler reduces (3.7) to

$$\frac{\partial^2 \eta}{\partial z^2}+\frac{2}{1+z}\frac{\partial \eta}{\partial z}=-\frac{2e^2 n_s r_s{}^2}{\varepsilon_o m_i u_B{}^2}\frac{\eta^{-1/2}}{(1+z)^2}. \qquad (3.8)$$

This is a non-linear second order differential equation which seems to have no simple analytic solution, and hence it must be solved using a power series. For the planar case it is known that the solution has the form $\eta = \beta\ z^m$ (Langmuir and Blodgett (1924)), so for spherical geometry it is assumed η will have a power series solution of the form

$$\eta=\beta z^m\left(1+a_1 z+a_2 z^2+a_3 z^3+\ldots\right), \qquad (3.9)$$

where β, m and a_i are unknown constants. Note that (3.9) conforms with the boundary conditions, since at $z = 0$ (the plasma-sheath boundary) $V = 0$, by definition, therefore $\eta = 0$. Differentiating (3.9) with respect to z, and including terms of up to z^2

$$\frac{\partial \eta}{\partial z}=\beta m z^{m-1}\left[1+\left(\frac{m+1}{m}\right)a_1 z+\left(\frac{m+2}{m}\right)a_2 z^2+\ldots\right], \qquad (3.10)(a)$$

and

$$\frac{\partial^2 \eta}{\partial z^2}=\beta m(m-1)z^{m-1}\left[1+\left(\frac{m+1}{m-1}\right)a_1 z+\frac{(m+2)(m+1)}{m(m-1)}a_2 z^2+\ldots\right]. \qquad (3.10)(b)$$

Multiplying both sides of (3.8) by $(z+1)^2$, and substituting for η using equation (3.9), and for $\partial\eta/\partial z$ and $\partial^2\eta/\partial z^2$ using (3.10)(a) and (b) yields

$$\beta m(m-1)z^{m-2}\left\{1+\left[\frac{m+1}{m-1}a_1+2\right]z+\left[\frac{(m+2)(m+1)}{m(m-1)}a_2+\frac{2(m+1)}{m-1}a_1+1\right]z^2\right\}$$
$$+\beta m z^{m-1}\left\{2+\left[\frac{2(m+1)}{m}a_1+2\right]z+\left[\frac{2(m+2)}{m}a_2+\frac{2(m+1)}{m}a_1\right]\right\}+O(z^3)$$
$$=\frac{2e^2 n_s r_s{}^2}{\varepsilon_o m_i u_B{}^2}\frac{\beta^{-1/2}z^{-m/2}}{\left(1+a_1 z+a_2 z^2\right)^{1/2}}. \qquad (3.11)$$

A binomial expansion to second order on the denominator in brackets on the right hand side of (3.11) gives

$$\left(1+a_1 z+a_2 z^2\right)^{-1/2} = 1-\frac{a_1}{2}z+\left(\frac{3a_1^{\,2}}{8}-\frac{a_2}{2}\right)z^2+\ldots \qquad (3.12)$$

Substituting (3.12) into (3.11) and rearranging coefficients of z gives

$$m(m-1)\beta\, z^{m-2}\left\{1+\left[\frac{m+1}{m-1}a_1+2+\frac{2}{m-1}\right]z+ \left[\frac{(m+1)(m+2)}{m(m-1)}a_2+\frac{2(m+1)}{(m-1)}\left(1+\frac{1}{m}\right)a_1+\frac{2}{m-1}+1\right]z^2\right\}$$

$$=\frac{2e^2 n_s r_s^{\,2}}{\varepsilon_o u_B^{\,2} m_i}\beta^{-1/2} z^{-m/2}\left[1-\tfrac{1}{2}a_1 z+\left(\tfrac{3}{8}a_1^{\,2}-\tfrac{1}{2}a_2\right)z^2\right]+O(z^3). \qquad (3.13)$$

For small z both sides of equation (3.13) are to the same order in z if $m-2=-m/2$, i.e., $m = 4/3$. The assumption of small z is justified since for most area ratios the bulk width is very much smaller than the electrode radii, therefore $x << r_s$. Only at very large area ratios, corresponding to small electrode radii, does $x \approx r_s$. By substituting m back into (3.13) and equating constants, β can be determined:

$$\beta^{3/2} = \frac{2e^2 n_s r_s^{\,2}}{\varepsilon_o u_B^{\,2} m_i}\frac{1}{m(m-1)} = \frac{9}{4}\frac{2e^2 n_s r_s^{\,2}}{\varepsilon_o u_B^{\,2} m_i}. \qquad (3.14)$$

Going back to equation (3.13) and comparing powers of z values for the coefficients a can be determined:

$$a_1 = -\frac{16}{15} \approx -1.067 \quad \text{and} \quad a_2 \approx \frac{38}{35} \approx 1.086 \qquad (3.15)$$

Substituting these values back into (3.9), the equation for η, in the limit of small z, is given by

$$\eta = \beta z^{4/3}\left(1-\frac{16}{15}z+\frac{38}{35}z^2+\ldots\right) \qquad (3.16)$$

An equation for the sheath voltage can be determined in terms of real variables by substituting for β, η and z in (3.16) and re-arranging to give

$$\left(\frac{2e}{m_i u_B^{\,2}}\right)^{3/2}(V_B - V)^{3/2}$$
$$= \frac{9}{4}\left(\frac{2e^2 n_s r_s^{\,2}}{\varepsilon_o m_i u_B^{\,2}}\right)\left(\frac{x}{r_s}\right)^2\left(1 - \frac{16}{15}\frac{x}{r_s} + \frac{38}{35}\left(\frac{x}{r_s}\right)^2 + O\left(\frac{x}{r_s}\right)^3\right)^{3/2}, \tag{3.17}$$

where $V_B = 1/2\, m_i u_B^{\,2} = 1/2\, kT_e$, the minimum energy with which ions enter the sheath.

At the electrode $x = s$, and $V = -V_S$. Using these boundary conditions in (3.17) and assuming $V_S >> V_B$, the sheath voltage can be determined as a function of maximum sheath width, current, and the radius of curvature

$$V_s \approx \frac{9}{4}\frac{e n_s u_B}{\varepsilon_o}\sqrt{\frac{m_i}{2e}}\, s^2\left(1 - \frac{16}{15}\left(\frac{s}{r_s}\right) + \frac{38}{35}\left(\frac{s}{r_s}\right)^2 + O\left(\frac{s}{r_s}\right)^3\right). \tag{3.18}$$

Using equation (3.3) to substitute for the current density at the sheath edge (3.18) can be written in the form:

$$j_s \approx \frac{4}{9}\varepsilon_o\sqrt{\frac{2e}{m_i}}\, V_s^{3/2} s^{-2}\left(1 - \frac{16}{15}z_s + \frac{38}{35}z_s^{\,3} + O\left(z_s^{\,3}\right)\right)^{-3/2}, \tag{3.19}$$

where $z_S = s/r_S$. Note that for the planar case (that is, when r_S approaches infinity) z_S approaches zero, and (3.19) reduces to the planar Child-Langmuir law. Since the current density is a function of position in the sheath, it is more convenient to write (3.19) in terms of the current, which is constant across the sheath. So using $i = 4\pi r_s^2 j_s$ (3.19) becomes:

$$i \approx \frac{16\pi}{9}\varepsilon_o\sqrt{\frac{2e}{m_i}}\, V_s^{3/2} z_s^{-2}\left(1 - \frac{16}{15}z_s + \frac{38}{35}z_s^{\,2} + O\left(z_s^{\,3}\right)\right)$$
$$= \frac{16\pi}{9}\varepsilon_o\sqrt{\frac{2e}{m_i}}\, V_s^{3/2} f(z_s). \tag{3.20}$$

3.1.2 *Time-averaged electron density in the sheath*

In the previous section the sheath equation was derived assuming that the sheath voltage and width remain constant and the electron density in the sheath is zero. However, when an rf voltage is applied to the electrode the voltage across the sheath

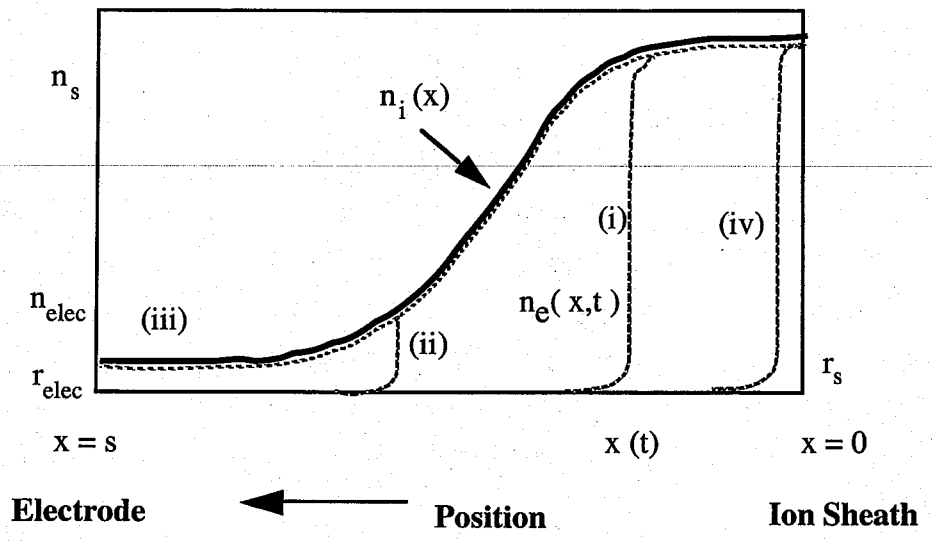

Figure 3.2 Schematic of the ion (solid line) and electron (broken line) density profiles. The step in the electron density represents the electron sheath edge and is represented at various phases of the cycle: (i) $\omega t = 0$ (ii) $\omega t = \pi/4$ (iii) $\omega t = \pi/2$ (iv) $\omega t = 3\pi/2$. The maximum extension of the electron sheath corresponds to the position of the ion sheath, r_s

varies periodically during the rf cycle. For applied frequencies in the range $\omega_{pi} > \omega_{rf} > \omega_{pe}$, where $\omega_{pi/e}$ is the ion/electron plasma frequency, the sheath voltage varies sinusoidally in time and once per cycle the voltage approaches zero and electrons can enter the sheath region (see Figure 4.2) . Defining the sheath edge as the position at which the electron density drops to zero, it is therefore obvious that this will also vary periodically with time, and is in fact found to do so in an approximately sinusoidally manner (analytic derivations of the sheath motion are presented by Lieberman (1988) and Raizer and Shneider (1992), and experimental measurements are given by Wood *et al* (1991)). The sheath edge can therefore be represented by a variable s(t), where $s = 0$ at the plasma-sheath boundary and $s = s_{max}$ at the electrode. In order to determine an expression for the sheath motion most analytic models assume that the electron density can be modelled as a step function with $n_e(x,t) = n_i(x)$ for $x < s(t)$ and $n_e(x,t) = 0$ for $x > s(t)$ (Meijer (1991), Lieberman (1988) and (1989b)). This is represented schematically in Figure 3.2.

In this section the effect of the periodic incursion of the electrons on the average charge density in the sheath is determined. The derivation of the sheath law in the previous section assumed that the time-averaged electron density in the sheath is zero. However, as discussed in the previous paragraph, this is not true for the case of rf sheaths and so the average charge density in the sheath can not be determined purely

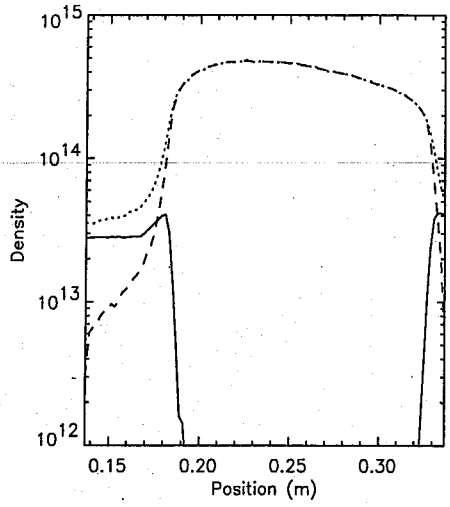

Figure 3.3 Results from the simulation showing ion density (dotted line), electron density (dashed line) densities and the difference $\overline{n}_i - \overline{n}_e$ (solid line) plotted as a function of position, averaged over the rf cycle.

from the ion density. Figure 3.3 is a simulation plot of the time-averaged densities in the plasma, showing the average electron density, the ion density, and the difference between the two – this amply demonstrates that the time-averaged charge density in the sheath is not given by the ion density.

In order to determine the effect of the sheath collapse on the dc sheath law calculated in the previous section, the effect of the regular incursion of electrons on the average charge density in the sheath must be used in the the derivation of the sheath equation. This can be accomplished by determining the relative fraction of the rf cycle for which each position in the sheath contains electrons. Results from the simulation indicate that the sheath collapses for approximately 15% of the rf cycle regardless of the plasma parameters. The effect of the electron incursion is calculated assuming that when the sheath is collapsed the electron density is equal to the ion density at all positions in the sheath.

Figure 3.4 (a) is a schematic diagram showing the motion of the electron sheath edge as a function of phase. The shading represents the regions where electrons are present (so the plasma is charge-neutral) and the blank area represents regions where electrons are excluded and which are therefore positively charged. For convenience the start of the rf cycle is chosen to be at the maximum sheath expansion. The variable ξ represents the average length of time during each cycle that electrons are excluded from position x, in effect representing a temporal sheath "width" as a function of position. Close to the electrode ξ is large, since electrons are excluded for most of the cycle. Conversely at the position of maximum sheath expansion, which electrons can diffuse to easily, ξ is small. Dividing ξ by π, gives the fraction of the rf cycle when there are no

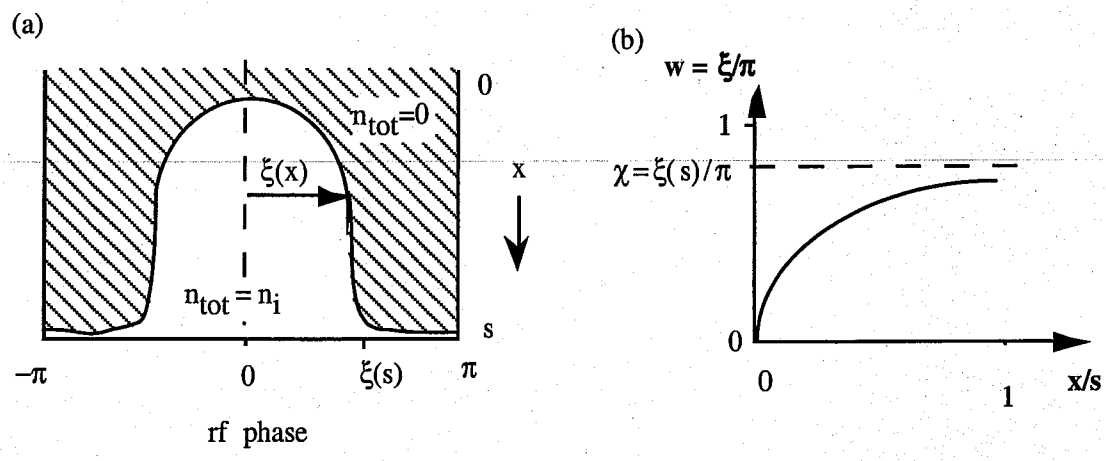

Figure 3.4 **(a)** The sheath width shown as a function of phase and position. In the sheath $n_{tot} = n_i$, outside it $n_{tot} = 0$ **(b)** dependence of w (normalised temporal sheath width) on x/s (normalised position), assuming parabolic sheath motion.

electrons at x. When electrons are present $\overline{n}_i - \overline{n}_e$ is equal to zero, otherwise it is equal to the ion density, so ξ/π is a measure of the ratio of the total and ion densities, averaged over the rf cycle

$$w(x) = \frac{\xi(x)}{\pi} = \frac{n_{tot}(x)}{n_i(x)}. \tag{3.21}$$

Assuming that the sheath motion is approximately parabolic, w can be written as a function of x:

$$w = \chi\sqrt{\frac{x}{s}}, \tag{3.22}$$

where χ is a constant of proportionality dependent on the fraction of the rf cycle for which the sheath does not exist at the electrode, i.e., when the sheath is completely collapsed. Figure 3.4 (b) shows w as a function of x. Taking results from simulations over the whole range of parameters it has been found that the sheath collapse time averages about 1.5 ns out of an rf period of 0.1 μs, and hence $\chi \approx 0.85$. For planar simulations, Vender (1990) finds the sheath collapses for 17% of the cycle, i.e. $\chi = 0.83$.

3.1.3 *Spherical rf sheath equation*

Using (3.21) and (3.22) derived in the previous section, the average total density in the sheath is given by

$$\overline{(n_i - n_e)} = \chi\, n_i(x)\sqrt{\frac{x}{s}}. \tag{3.23}$$

Substituting equations (3.23) and (3.6) into Poisson's equation (3.1), the differential sheath equation is found to have the form

$$\frac{\partial^2 V}{\partial x^2} + \frac{2}{r_s + x}\frac{\partial V}{\partial x} = -\frac{en_s\chi\sqrt{x/s}}{\varepsilon_o\left(1+\dfrac{x}{r_s}\right)^2\sqrt{1-\dfrac{2eV(x)}{m_i u_B{}^2}}}, \tag{3.24}$$

which is similar to equation (3.7), but with an extra term $\chi\sqrt{x/s}$. Using normalised variables η and z and solving as for the dc sheath, the power series solution for η is given by

$$\eta = \beta z^{5/3}\left(1 - \frac{10}{9}z + \frac{2885}{2511}z^2 + \ldots\right), \tag{3.25}$$

where

$$\beta^{3/2} = \left(\frac{9}{10}\right)\left(\frac{2e^2 n_s r_s{}^2 \chi}{\varepsilon_o m_i u_B{}^2\sqrt{s}}\right).$$

Re-writing (3.25) the potential at the electrode, V_s, is given by

$$\begin{aligned} V_s^{3/2} &= \frac{9}{10}\frac{2e^2 n_s r_s^{5/2}\chi}{\varepsilon_o m_i u_B{}^2\sqrt{s}}\left(\frac{m_i u_B{}^2}{2e}\right)^{3/2}\left(\frac{s}{r_s}\right)^{5/2}\left(1-\frac{10}{9}z+\frac{2885}{2511}z^3+\ldots\right)^{3/2} \\ &= \frac{9}{40\pi}\sqrt{\frac{m_i}{2e}}\chi\frac{4\pi r_s{}^2(en_s u_B)}{\varepsilon_o}\left(\frac{s}{r_s}\right)^2\left(1-\frac{10}{9}z+\frac{2885}{2511}z^3+\ldots\right)^{3/2}. \end{aligned} \tag{3.26}$$

Introducing $i = 4\pi r_o{}^2(en_o u_B)$ and re-arranging (3.26) the sheath equation can be written in the form

$$i = \frac{40\pi}{9}\sqrt{\frac{2e}{m_i}}\frac{\varepsilon_o}{\chi}V^{3/2}\left(\frac{r_s}{s}\right)^2\left(1-\frac{10}{9}z+\frac{2885}{2511}z^3+\ldots\right)^{-3/2},$$
$$= \frac{40\pi}{9}\sqrt{\frac{2e}{m_i}}\frac{\varepsilon_o}{\chi}V^{3/2}\left(\frac{r_s}{s}\right)^2(1+z)^{5/3}, \qquad (3.27)$$

where

$$\left(1-\frac{10}{9}z+\frac{2885}{2511}z^2+\ldots\right)^{-3/2} \approx 1-1.667z+0.591z^2+\ldots$$
$$= (1+z)^{5/3}+0.036z^2+O(z^3)$$

Replacing the normalised variable z gives $(1 + z)^{5/3} = (1 + s/r_s)^{5/3} = \left[(r_s + s)/r_s\right]^{5/3}$. At the outer electrode $r_s = r_b - s$ and at the inner $r_s = r_a + s$, hence the radius of the sheath r_s can be replaced by $r_s = r_{elec} \pm s$, where r_{elec} is the electrode radius and the sign depends on which electrode sheath is being calculated. Substituting back into equation (3.27) gives an expression for the sheath current in terms of the electrode radius

$$i = \frac{40\pi}{9}\sqrt{\frac{2e}{m_i}}\frac{\varepsilon_o}{\chi}V^{3/2}\left(\frac{r_{elec}}{s}\right)^2\left(\frac{r_{elec}\pm s}{r_{elec}}\right)^{5/3}, \qquad (3.28)$$

Figure 3.5 shows the values of the ion currents to the live and grounded electrodes calculated from (3.28), using $\chi = 0.85$, plotted for different area ratios and applied voltages. Values of V and s were determined from the simulations. Plotted on the same graph is the ion current determined from an equation for the bulk derived in Section 3.3.5, and the actual ion currents measured in the simulation. Agreement between the simulation and both sets of calculated currents is very good over most of the range of area ratios and voltages. The largest discrepancies occur at very low currents. This could partially be an effect of numerical noise in the simulation since at currents of ~0.5 A, fluctuations in the current are of the same order as the average value. The relative errors in the sheath widths and potentials from the simulation also increase at these low magnitudes and can lead to discrepancies.

A final point to note is that the ion currents at the live and grounded electrodes are not necessarily equal, since only the total current is required to be the constant across the plasma. However, since there can be no net accumulation of charge on the electrodes the total flux of electrons and ions to each electrode in one cycle must be equal.

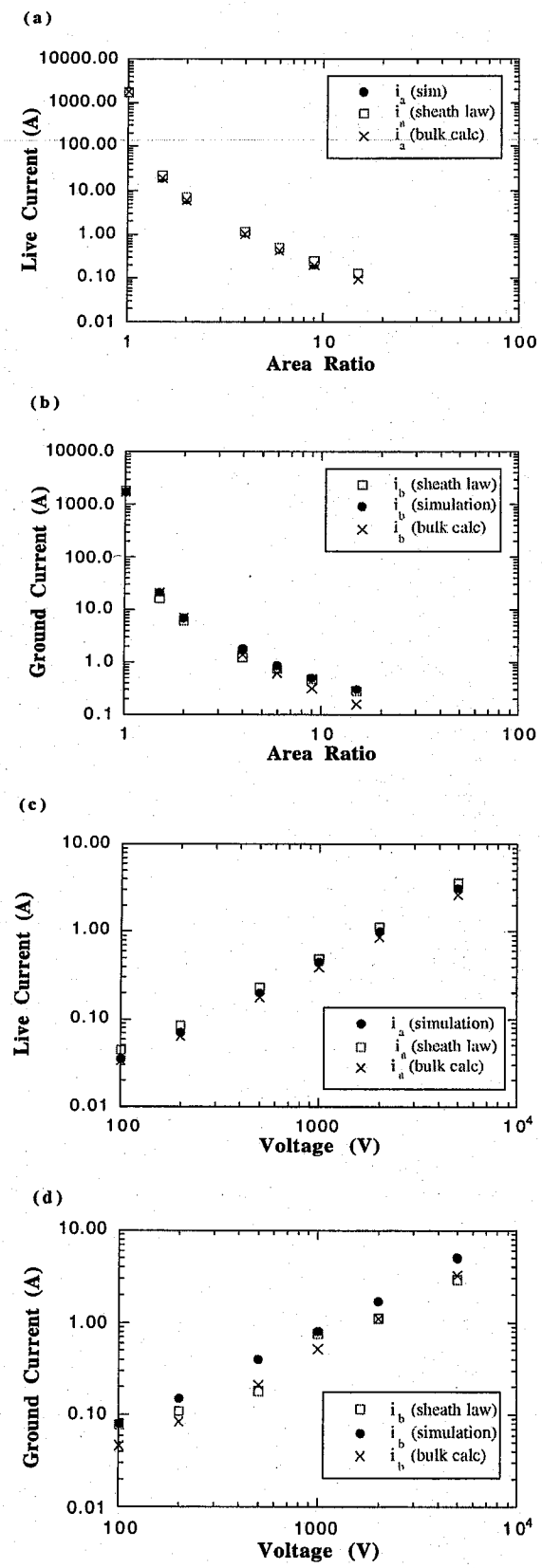

Figure 3.5 Ion currents from the simulation plotted in comparison with theoretical values calculated from the sheath (3.28) and bulk (3.50) equations as functions of area ratio and applied voltage. Note that i_a is the current to the live electrode and i_b to the grounded electrode.

3.2 Determining bulk plasma potentials

As mentioned in the introduction to this chapter the results from the PIC simulations cannot be compared to analytic models published in the literature. Predominantly this is because these models are derived for planar, not spherical, coordinate systems and assume that ion transport in the bulk is dominated by collisions with neutrals. Although this is correct for most experimental conditions the simulation results with collisionless ions cannot be directly compared to results from these models since ion-neutral collisions have a profound effect on the average ion energies in the plasma, the currents, and the density and potential distributions. Hence potential, density and particle energy distributions in the bulk are determined using a modified form of the analytic kinetic theory originally developed by Langmuir and Tonks (1929). Results from this model are compared to the PIC simulations in Section 3.2.6; and to numerical results from Bissell, Johnson and Stangeby (1989) in Section 3.2.8.

3.2.1 Derivation of the bulk potential equation

As in the sheath derivation, Poisson's equation (3.1), is used to determine the potential distribution in the bulk. A schematic of the bulk distribution is shown in Figure 3.6. At a position r_o the average potential reaches a peak, so r_o is used as the zero position – ions generated at positions greater than r_o will drift in the positive direction toward the grounded electrode, while ions at positions less than r_o will drift in the

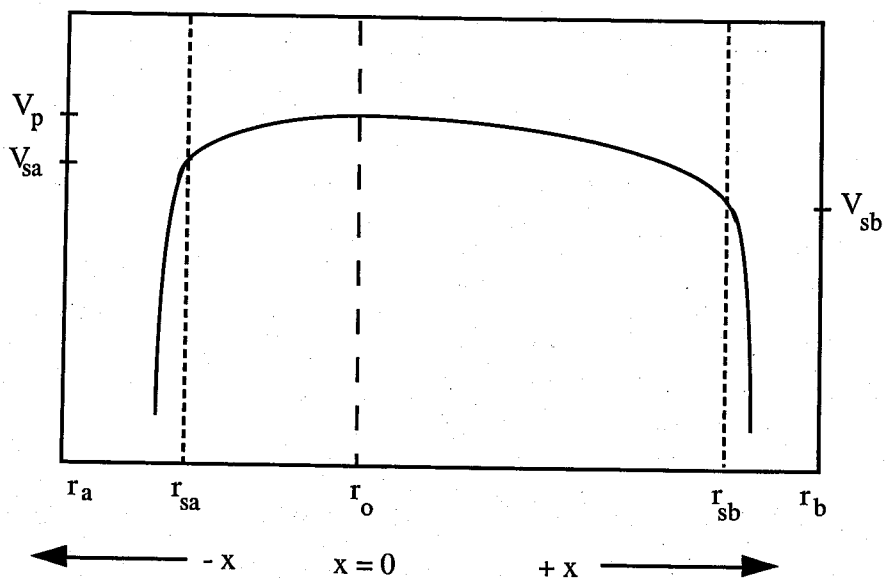

Figure 3.6 Schematic of average potential across the plasma. The live electrode is at the left and the grounded electrode at the right.

negative direction toward the powered electrode. Hence in the following theory the bulk is divided into the positive and negative regions – the negative region being closest to the live electrode and the positive to the grounded electrode. The following equations are derived for the positive region of the bulk – that is from r_o to r_{sb}, the position of the ground sheath edge, and then generalised for both directions. As will be shown later it is convenient to treat the two halves of the plasma separately due to the different conditions which are generated at the powered and grounded electrodes.

Assuming that the bulk fields are small and that electron-neutral collisions quickly thermalise the high energy electrons, the electrons can be assumed to have a Maxwellian distribution, and so will have a well-defined temperature. The average electron density as a function of position is therefore given by

$$n_e(r) = n_o e^{-e\phi(r)/kT_e}, \tag{3.29}$$

where n_o is the density at r_o and $\phi(r) = V_p - V(r)$ is the difference in potential between r_o and r.

The ion density is determined by balancing the creation rate due to ionisation with the loss rate to the sheaths. The potential on each side of r_o decreases monotonically from the peak potential, V_p, toward the sheath-edge potentials, V_s, and so the ions are accelerated from the position they are created out toward the electrodes at speeds determined by the average local fields. If the number of ions created per second per unit volume at a position z (for $z > r_o$) is N_z, then the density at a further position r, of ions which have travelled from z, is given by $N_z\, 4\pi z^2\, dz/4\pi r^2\, u_z$, where u_z is the velocity gained by the ions in travelling from z to r. Ions created at every position, $z < r$, will contribute to the total density at r, which is therefore given by:

$$n_i(r) = \frac{1}{r^2}\int_{r_o}^{r} \frac{N_z z^2}{u_z(r)}\, dz. \tag{3.30}$$

Substituting (3.29) and (3.30) into equation (3.1) and using $r = r_o + x$, Poisson's equation can be re-written in the form

$$\nabla^2\phi(x) - \frac{en_o}{\varepsilon_o} e^{-e\phi(x)/kT_e} + \frac{e}{\varepsilon_o (r_o + x)^2}\int_0^x \frac{N_z (r_o + z)^2}{u_z}\, dz = 0. \tag{3.31}$$

Since the electron temperature is assumed to be constant, the ionisation rate per electron, ν_I will also be constant. Assuming, furthermore, that the creation rate for ions is proportional to the electron density, so that N_z , the number of ions generated at z per second, is proportional to $n_e(z)$, the electron density at z, then it follows that

$N_z = \upsilon_I n_e(z) = \nu_I n_o e^{-e\phi(z)/kT_e}$. If ions are created at rest at position z and they make no collisions, then their velocity at r is given by $u_z(r) = \sqrt{\frac{2kT_e}{m_i}}(\eta_r - \eta_z)^{1/2}$, where η_r and η_z are the normalised potentials at r and z, with $\eta = \frac{e\phi}{kT_e}$. Equation (3.31) can then be simplified, by assuming quasi-neutrality in the bulk so that $\nabla^2 \approx 0$. Substituting for N_z and u_z in equation (3.30)

$$e^{-\eta} - \frac{\nu_I}{(r_o + x)^2}\sqrt{\frac{m_i}{2kT_e}}\int_0^x \frac{e^{-\eta_z}(r_o + z)^2}{\sqrt{\eta - \eta_z}}dz = 0. \qquad (3.32)$$

Following the method used by Tonks and Langmuir (1929), equation (3.32) can be solved by changing the independent variable from η to x and introducing the change of variable:

$$\eta = \rho^2, \qquad \eta_z = \rho_z{}^2 \qquad \text{and } \rho_z = \rho\sin\theta. \qquad (3.33)$$

This gives an equation of the form

$$e^{-\eta} = \frac{\gamma}{(r_o + x)^2}\int_0^{\frac{\pi}{2}} e^{-\rho_z{}^2}(r_o + z)^2 \frac{dz}{d\rho_z}d\theta. \qquad (3.34)$$

where $\gamma = \frac{\nu_I}{\sqrt{2}\,u_B}$ is a new constant with dimensions m^{-1}.

Equation (3.34) is quite difficult to solve since the functional dependence of x on ρ is unknown. However, if it is assumed that x can be expressed as a power series in ρ, i.e.,

$$x = a_o + a_1\rho + a_2\rho^2 + a_3\rho^3 + ..., \qquad (3.35)$$

then the integral in (3.34) can also be expressed as a power series and by equating terms of ρ, the coefficients of (3.35) can be determined. Using the boundary condition $\rho = 0$ at $x = 0$ gives $a_o = 0$. To determine the rest of the coefficients each term in the integral in (3.35) is expanded in terms of up to ρ^3

$$e^{-\rho_z} = 1 - \rho_z{}^2 + ...$$

$$(r_o + z)^2 = r_o{}^2 + 2r_o a_1\rho_z + (2r_o a_2 + a_1{}^2)\rho_z{}^2 + 2(r_o a_3 + a_2 a_1)\rho_z{}^3 + ...$$

$$\frac{\partial z}{\partial \rho_z} = a_1 + 2a_2\rho_z + 3a_3\rho_z{}^2 + 4a_4\rho_z{}^3 + ... \qquad (3.36)$$

Multiplying each side of (3.35) by $(r_o + x)^2$ and expanding both sides in terms of ρ, using the expansions given in (3.36), the bulk equation can be re-written in the form

$$\begin{aligned} r_o^2 + 2a_1 r_o \rho + \left(2a_2 r_o + a_1^2 - r_o^2\right)\rho^2 + 2\left(r_o a_3 + a_1 a_2 - a_1 r_o\right)\rho^3 + \ldots \;, \\ = \gamma \int_0^{\pi/2} \left[b_o + b_1 \rho \sin\theta + b_2 (\rho \sin\theta)^2 + b_3 (\rho \sin\theta)^3 + \ldots\right] d\theta, \\ = \gamma \left[\frac{\pi}{2} b_0 + b_1 \rho + \frac{\pi}{4} b_2 \rho^2 + \frac{2}{3} b_3 \rho^3 + \ldots\right], \end{aligned}$$

where

$$\begin{aligned} b_o &= a_1 r_o^2, \\ b_1 &= 2r_o(a_1^2 + a_2 r_o), \\ b_2 &= 6a_1 a_2 r_o + a_1^3 + 3a_3 r_o^2 - a_1 r_o^2, \\ b_3 &= 8a_1 a_3 r_o + 4a_1^2 a_2 + 4a_2^2 r_o + 4a_4 r_o^2 - 2a_1^2 r_o - 2a_2 r_o^2. \end{aligned} \tag{3.37}$$

Equating coefficients of ρ from each side of equation (3.37) gives values for a_i of

$$\begin{aligned} a_1 &= \frac{2}{\pi\gamma}, \\ a_2 &= \frac{2}{\pi\gamma^2 r_o}\left(1 - \frac{2}{\pi}\right), \\ a_3 &= \frac{-8}{3\pi^2\gamma^3 r_o^2}\left(1 - \frac{3}{\pi}\right) - \frac{2}{3\pi\gamma}, \\ a_4 &= \frac{-1}{\pi^2\gamma^4 r_o^3}\left(3 - \frac{56}{3\pi} + \frac{32}{\pi^2}\right) + \frac{1}{\pi\gamma^2 r_o}\left(\frac{8}{3\pi} - 1\right). \end{aligned} \tag{3.38}$$

Substituting the coefficients determined in (3.38) into equation (3.34) and converting back from ρ to η gives x as a function of the normalised potential. Note that (3.34) is calculated only in the positive direction (ie from r_o to the outer electrode). In the negative direction x has the form

$$x_- = a_1\rho - a_2\rho^2 + a_3\rho^3 - a_4\rho^4 + \ldots \tag{3.39}$$

The full solution for both directions, evaluating the numerical coefficients to four significant figures, is therefore

$$\begin{aligned} x_\pm = \frac{2}{\pi\gamma}\eta^{1/2}\Bigg\{1 \pm \frac{0.3634}{\gamma r_o}\eta^{1/2} - \left(\frac{0.0191}{(\gamma r_o)^2} + 0.3333\right)\eta \\ \pm \left(\frac{0.0478}{(\gamma r_o)^3} - \frac{0.0756}{\gamma r_o}\right)\eta^{3/2} + \left(\frac{0.0117}{(\gamma r_o)^4} + \frac{0.0743}{(\gamma r_o)^2} - 0.0333\right)\eta^2 + \ldots\Bigg\}. \end{aligned} \tag{3.40}$$

Equation (3.40) gives the position in the bulk as a function of the normalised potential (which is the inverse of the conventional functionality). As x is measured from the mid-point of the plasma, r_o, the radial position in the bulk is determined by $r_\pm = r_o \pm x_\pm$. For comparison with the spherical bulk equation, the solution for the planar (symmetric) case is

$$x_\pm = x_{plan} = \frac{2}{\pi\gamma}\left(1 - \frac{1}{3}\eta - \frac{1}{30}\eta^2 - \frac{1}{210}\eta^3\right). \tag{3.41}$$

Note that in this case there is no dependence on r_o since the system is symmetric. The symmetry in the planar case dictates that the bulk width, the distance between r_o and the sheath edges, is the same for both negative and positive regions of the plasma. This is not the case for the asymmetric system, as will be shown in the next section.

3.2.2 Sheath-edge potential calculation

In order to use (3.40) or (3.41) to determine the potential distribution in the bulk it is necessary to know the normalised potential at the sheath edges, $\eta_{s\pm}$. This can be determined from the value of η at which $dr/d\eta \to 0$, since this is the position at which the potential gradient starts to become extremely large, indicating the sheath edge. The spherical equations must be solved numerically to determine this value, since there is no simple analytic solution. The symmetric planar case, on the other hand, can be solved analytically to give the normalised potential at the sheath edge, η_p, and the distance between the sheath edge and the centre of the plasma, x_p. Differentiating equation (3.41) and equating the result to zero gives

$$\left.\frac{dx}{d\eta}\right|_{\eta=\eta_p} = \frac{2}{\pi\gamma}\eta_p^{-1/2}\left(1 - \tfrac{1}{3}\eta_p - \tfrac{1}{30}\eta_p^{\,2} - \tfrac{1}{210}\eta_p^{\,3}\right) = 0. \tag{3.42}$$

Solving (3.42) for η_p and substituting back into equation (3.41), gives the solution for the planar system

$$\eta_p = 0.857 \quad \text{and} \quad x_p = \frac{0.405}{\gamma}. \tag{3.43}$$

To test the accuracy of equation (3.43) the calculated value for the total bulk width is compared to the simulation for the symmetric system. Assuming an electron temperature of 3.5 eV the ionisation rate is $\nu_I = 1.4\text{x}10^5\ \text{s}^{-1}$ and the ion acoustic velocity $u_B =$

1.83×10^4 ms^{-1}, and therefore $\gamma = 5.36$ m^{-1}. Hence $d = 2x_s = 2 \times 0.405/\gamma = 0.15$ m, which is within 10% of the simulation value of $d = 0.14$ m.

As mentioned previously it is not possible to calculate the spherical values for the normalised sheath potential, η_s, analytically. However for systems which are reasonably close to planar an approximate solution can be obtained by expanding around the planar solution. Hence an equation is obtained of the form

$$\eta_{s\pm} = \eta_o \pm \frac{c_\pm}{\gamma_\pm r_o} + O\left(\frac{1}{r_o^2}\right), \tag{3.44}$$

where c is a constant, and $\pm$ refers to the relevant region of the plasma. The constants have been determined by fitting to results from the simulation and equation (3.40), giving the values $c_+ = 0.55$, and $c_- = 0.2$. In Figure 3.7 simulation, numerical and fitted results for η_s are plotted as functions of area ratio, voltage and pressure.

From Figure 3.7(a) it can be seen that the normalised sheath voltage in the negative region is fairly independent of area ratio, while the positive sheath voltage increases by a factor of 2 over the range of area ratio. The simulation results show quite a large degree of scatter, especially for the negative region, although there is good agreement between the numerically determined potentials from (3.40) and those fitted using (3.44). The scatter in simulation values of η_- is probably due to the steep potential gradient at the live sheath edge - an error of a few millimetres in determining the sheath position can result in an error in the measured potential of several tens of volts. For the numerical results it is conversely the negative region which will have the highest degree of error, since the potential slope tends to be more gradual (see $\alpha = 15$ in Figure 3.12(c)) which can make it difficult to determine the position at which $dx/d\eta = 0$. This effect turns out to be particularly important at high pressures and frequencies, since the potential gradients are often very shallow for these cases.

Figure 3.7(b), the normalised potential as a function of voltage, shows that both positive and negative sheath potentials are fairly independent of the applied voltage over the whole range. The simulation results for η_- again show a lot of scatter but agreement between the fitted and numerical results is good. On the whole it can be said that the fitted results follow the correct trend and provide a simple and useful means of determining the sheath edge potential.

However, as pressure is increased, as shown in Figure 3.7(c), the discrepancy between the behaviour of the simulated and calculated results becomes very large. The simulation results, for both negative and positive sheath potentials, decrease with increasing pressure. As the normalised potential that is plotted ($\eta = V/kT_e$), this implies

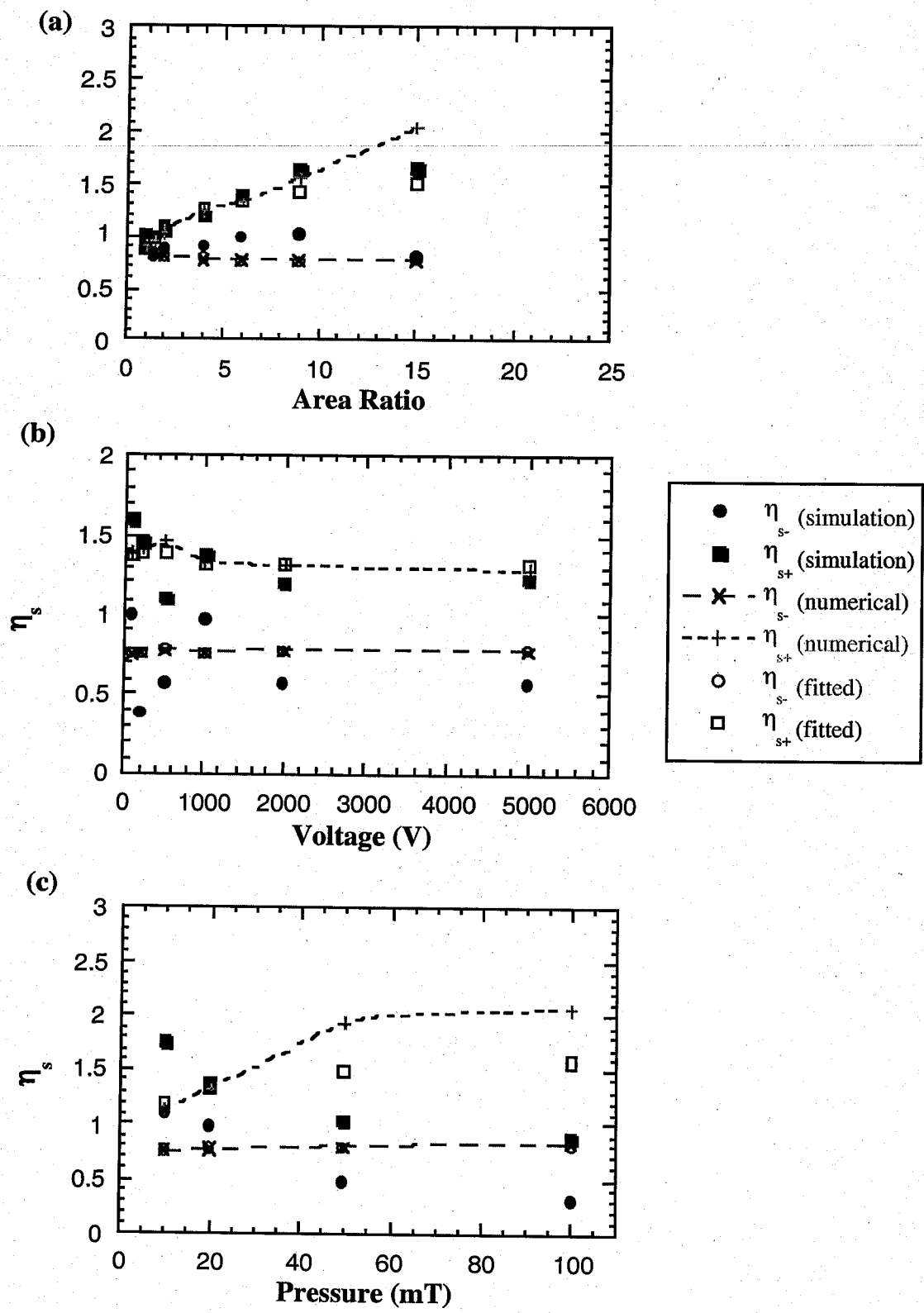

Figure 3.7 The normalised sheath potential for negative (η_{s-}) and positive (η_{s+}) sheath edges showing simulation data (filled symbols) and numerical solutions to equations (3.40) (crosses) and equation (3.44) (hollow symbols), as functions of **(a)** area ratio, **(b)** applied voltage and **(c)** pressure. A line is fitted to the numerical results as a guide for the eye.

that in the simulation the potential drop across the bulk region decreases relative to the electron temperature, with increasing pressure. Conversely, both the fitted and the numerically calculated potentials increase with increasing pressure, indicating the opposite behaviour. Further, there is increasing disagreement between numerical and fitted results with increasing pressure. The difference between simulation and theory is most likely due to the substantial gradients in the average electron energy across the bulk occuring at higher pressures. This effectively means that the electrons do not have a single well-defined temperature in the bulk region, as assumed in deriving the bulk equations (3.40) and (3.41). Electron temperature gradients in the bulk are discussed in more detail in Section 3.4.

3.2.3 *Bulk width*

To first introduce a point of terminology: when reference is made to the bulk width the distance between r_o and the sheath position is meant, rather than the total body of the plasma , and so for the asymmetric system the negative and positive bulk widths will generally be different. When the distance across the plasma from sheath to sheath is referred to it is specifically called the *total* bulk width. Using equation (3.40) the bulk widths can be determined once values for the normalised sheath potentials are known. Simulation results for the bulk widths in the positive and negative directions, x_- and x_+, are plotted in Figure 3.8 as functions of (a) area ratio, (b) voltage and (c) pressure.

Figure 3.8 (a) shows that the negative bulk width decreases and the positive bulk width increases with area ratio in such a way that the total bulk width remains approximately constant. Figure 3.8(b) shows that both positive and negative bulk widths, and hence the total width, are essentially independent of the applied voltage. However, from Figure 3.8(c) it can be seen that the total width increases with pressure. This is because as the pressure increases so also does the density, and since the sheath width is inversely proportional to density, the bulk width must consequently increase. Hence the total bulk width is approximately constant as a function of area ratio and voltage, and depends only on pressure (and frequency, although this is not plotted).

Results from planar parallel plate simulations (Vender (1990); Surrendra (1991)) also show that the sheath width remains constant with increasing voltage. This is an unexpected result since a simplistic consideration of the sheath equation (3.19) would indicate that the sheath width should increase with increasing applied voltage. However it turns out that the particle density increases with voltage approximately as $V^{3/2}$, roughly cancelling the effect of the voltage on the sheath and so the sheath width stays constant.

The reason that the total sheath width remains constant for changing area ratio has a more complex explanation, since the live and ground sheath widths have a non-linear

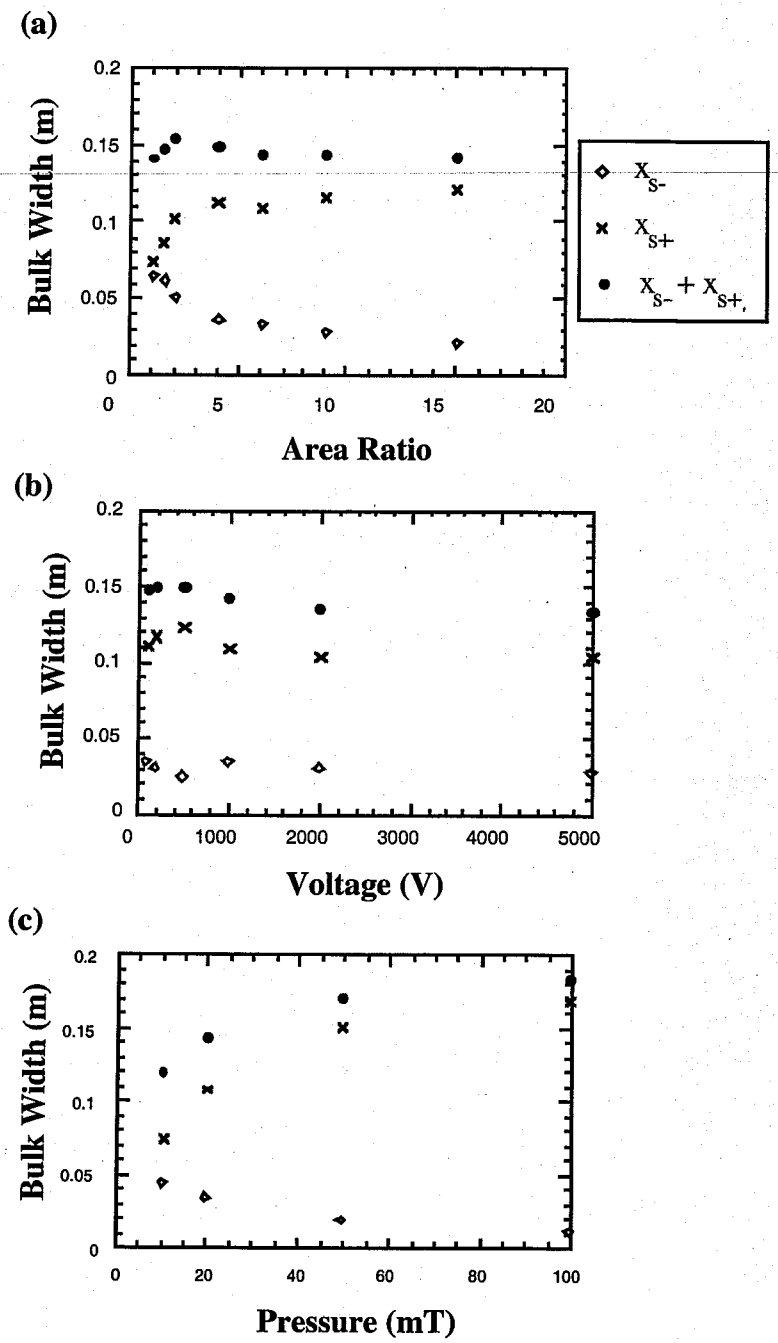

Figure 3.8 Negative bulk width, x_{s-}, positive bulk width, x_{s+}, and the total width as functions of **(a)** area ratio, **(b)** voltage and **(c)** pressure

dependence on the area ratio. However results from the simulation show that the average power per particle as a function of area ratio is constant (which covers a range of over six decades in the average power), indicating that the energy required per particle to maintain the electron and ion processes in the system must be independent of area ratio. The average electron energy is constant since T_e is found to depend only on the pressure, which is held constant as area ratio is changed. (Note that this is the *average* electron

energy - electrons in the sheaths can be accelerated to high energies which are very dependent on sheath voltage/width (see Chapter 4) but their densities are very low and so they contribute little to the average energy). The average ion energy on the other hand depends entirely on the sheath parameters, since ions in the bulk have energies of around 0.025 eV, so even if only 1% of the ions are in the sheaths they still contribute to nearly 100% of the total energy. The sheath potential determines the total energy each individual ion can gain, and the ratio of the total sheath width to the electrode separation is, to first order, a measure of the fraction of energetic ions in the plasma. So the product of the total sheath width and the voltage is roughly equal to the average energy per ion and from the previous arguments must therefore be constant. Hence for constant applied voltage the total sheath width must also be constant. As the average power per particle increases linearly with applied voltage a similar argument can be applied to also explain constant bulk width as a function of applied voltage. Note that this simple explanation ignores the effects of spatial variation in ion density and the spherical geometry.

3.2.4 Average Electron Temperature

In order to calculate the potential distribution in the bulk it is necessary to know the electron temperature - this gives the value of γ needed to calculate η_s and is also used to re-scale the normalised potentials back to real values. In the derivation of the bulk equations in Section 3.2.1 it is assumed that the electron temperature is constant across the bulk. For the symmetric case at low pressures the temperature gradients are small and so this is essentially true, therefore the average electron temperature should depend only on the neutral pressure and the volume in which ionisation takes place within the plasma. This can be seen by rearranging equation (3.43) to obtain

$$\gamma = \frac{\nu_I}{\sqrt{2}\,u_b} = \frac{0.405}{x_o}, \tag{3.45}$$

where, as previously noted, ν_I and u_B are functions of electron temperature. The equation for the ionisation rate, ν_I, is simply

$$\nu_I = N_n\, \sigma(\varepsilon)\, u_{th}, \tag{3.46}$$

where $u_{th} = \sqrt{\frac{8ekT_e}{\pi m_e}}$ is the average thermal electron velocity, N_n is the number of neutrals, and σ is the energy dependent cross-section. By convolving a Maxwellian electron distribution for temperatures up to 60 eV with the ionisation cross-section for

hydrogen, the average cross-section can be expressed as a function of kT_e. Appendix A details the full derivation, according to which the cross-section can be written as $\sigma(kT_e) = \sigma_o e^{-\varepsilon_{ion}/kT_e}$, where σ_O = 8.2x10^{-21} m^2 and ε_{ion} = 13.6 eV. Substituting for the ionisation rate and the ion acoustic velocity, (3.45) can be rewritten in terms of kT_e:

$$kT_e = \frac{\varepsilon_{ion}}{\ln\left(N_n \frac{d}{0.81\sqrt{2}}\right) + K}, \qquad (3.47)$$

where $K = \ln\left(\sigma_o \sqrt{\frac{8m_i}{\pi m_e}}\right) = -42.03$ for hydrogen plasmas.

For a background pressure of 20 mTorr N_n = 6.4x10^{20} m^{-3}; and from Section 3.2.3 d = 0.147 m, essentially independent of area ratio and voltage. Therefore (3.47) gives a value for the electron temperature of kT_e = 3.5 eV, independent of area ratio and voltage. It will however have some pressure and frequency dependence, since d is not independent of these parameters. From simulation results the average electron energy is approximately constant for all area ratios and applied voltages and is equal to 5.5 eV. The simulation has 3 velocity components, therefore asuming a Maxwellian distribution and using ε_{av} = 3/2 kT_e, the temperature is 3.7 eV.

Equation (3.47), valid for planar systems, determines a single electron temperature for the entire bulk region and is simple to calculate. However, results from the simulation show that the average electron energy in the bulk can be quite strongly dependent on position, and that the electron distribution can deviate substantially from a Maxwellian distribution under certain conditions. In Figure 3.9 the electron energy, averaged over the rf cycle, is plotted as a function of position in the plasma (the live electrode is at 0 and the grounded electrode at position 0.2 m). Plots are shown for α= 1, 2, 6, and 15, where α is the electrode area ratio. The plots show that the average energy is high in the sheath region with a very steep gradient at the position of the maximum sheath edge, and decreases rapidly to a more constant value in the bulk. Both the peak energy in the sheath and the bulk value increase with increasing area ratio. The high electron energies in the sheath are due to interaction with the moving sheath edge, this phenomena is discussed further in Chapter 4.

Examining the bulk energy distribution on an expanded scale in 3.9(b) it can be seen that even in the bulk there is a noticeable gradient in the average electron energy, especially at larger area ratios. Clearly the electron temperature does not have a single well-defined value, or even two distinct values for the different bulk regions, in fact there is a gradient across the entire bulk region, sloping down from the live to the grounded sheath. This indicates that the assumption of a uniform constant Maxwellian electron

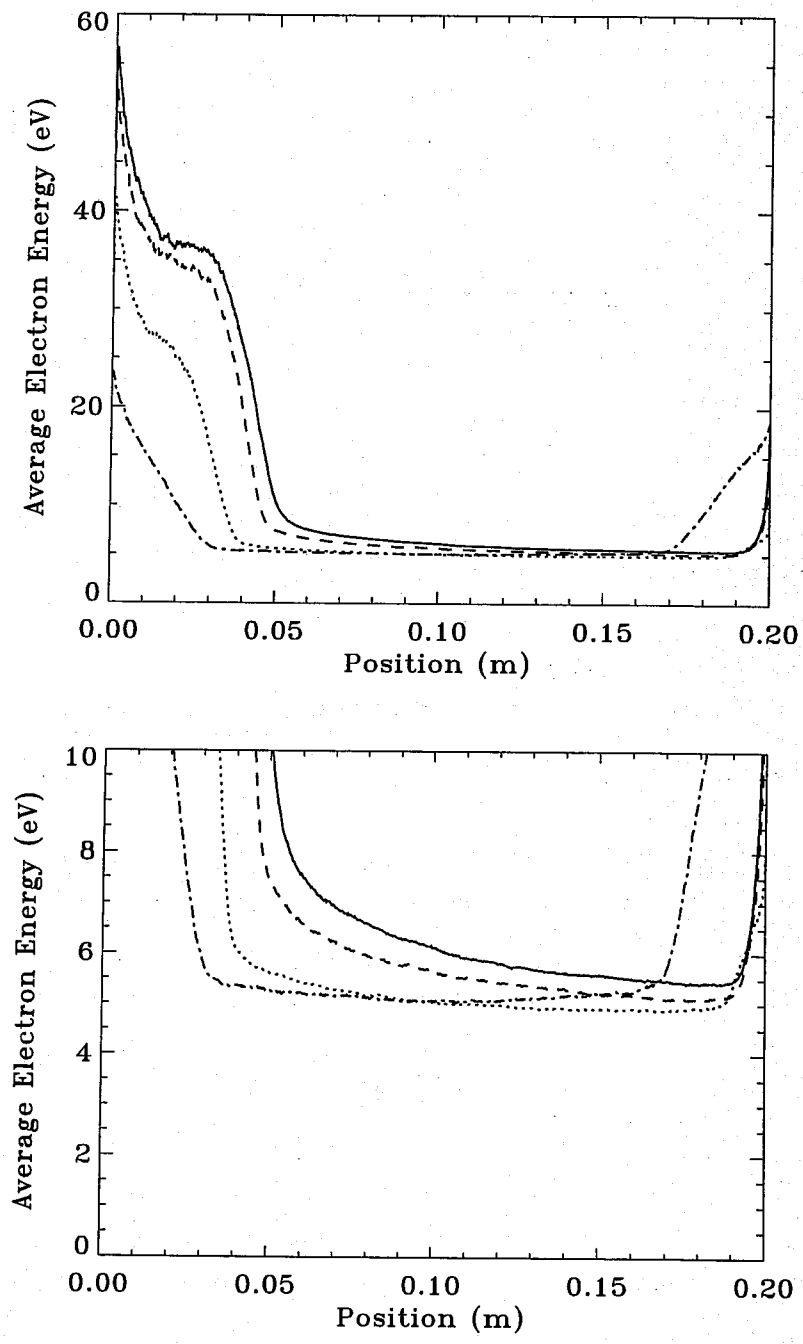

Figure 3.9 Simulation results for the time-averaged electron energy as a function of position at α=15 (solid line), 6 (dashed line), 2 (dotted line) and 1 (dash-dot line). Note in the second plot the vertical scale is expanded to show the bulk energies more clearly.

temperature in the initial derivation is too simplistic. However, for plasma parameters where the gradients are not *too* large a reasonable first approximation is to model the temperature gradient using two different average temperatures for the positive and negative regions in the bulk calculation. Including a temperature gradient in the bulk would require a numerical solution of the bulk equation (3.31), and so would not give simple analytic expressions for the plasma parameters which was a major aim in deriving this model. Using *two* temperatures in some measure compensates for assuming that kT_e is independent of position in the original derivations in section 3.2.1, while maintaining the simpler equation. In practice this turns out to work well except for the high pressure limit of the parameter range where temperature gradients are large.

Conservation of charge is used to derive an expression for the two bulk temperatures, noting that the creation rate in each region of the plasma must equal the loss rate to the corresponding electrode. Hence the ionisation rate per electron multiplied by the integral of the density over the volume of that region of plasma must equal the total ion flux at the corresponding sheath edge

$$\int_0^{x_s} \nu_I \, n(z) 4\pi (r_o \pm z)^2 dz = 4\pi (r_o \pm x_s)^2 n(x_s). \tag{3.48}$$

Assuming that the density distribution in the bulk is parabolic, the density can be written as a function of position x : $n(x) = n_o\left[1-(1-\zeta)(x/x_s)^2\right]$, where $\zeta = \mathrm{e}^{-\eta_s}$, η_s is the normalised potential at the sheath edge and n_o is the peak density (see Section 3.2.6). Substituting this expression into equation (3.48) together with (3.46) for the ionisation rate gives:

$$N_n \sigma_o e^{-\varepsilon_{ion}/kT_e} \sqrt{\frac{8ekT_e}{\pi m_e}} \int_0^{x_s} n_o\left[1-(1-\zeta)(z/x_s)^2\right]\left[r_o \pm z\right]^2 dz = (r_o \pm x_s)^2 n_o \zeta \sqrt{\frac{kT_e}{m_i}}$$

$$N_n \sigma_o e^{-\varepsilon_{ion}/kT_e} \sqrt{\frac{8}{\pi m_e}}\left[\frac{r_o^2}{3}(2+\zeta)x_s \pm \frac{r_o}{2}(1+\zeta)x_s^2 + \mathrm{O}(x_s^3)\right] = \frac{\zeta}{\sqrt{m_i}}\left(r_o^2 \pm 2r_o x_o + x_o^2\right)$$

Rearranging this equation, and assuming that $x_s^2/r_o^2 \to 0$ (i.e., the bulk width is smaller than the radial distance to the centre - true for all conditions presented in this thesis), then kT_e can be written in the form

$$kT_{e\pm} = \frac{\varepsilon_{ion}}{\ln\left(\frac{N_n}{\zeta_\pm} x_{s\pm} \frac{\frac{1}{3}(2+\zeta_\pm) \pm (1+\zeta_\pm) x_{s\pm}/r_o}{1 \pm 2x_{s\pm}/r_o}\right) + K}. \tag{3.49}$$

The results from equation (3.49) are plotted in Figure 3.10 in comparison with simulation results. The straight line is the temperature predicted by the planar equation, which is close to the simulation temperatures in the positive region of the bulk, but is often very different from those in the negative region. Figure 3.10 (a) is a plot of the temperature as a function of area ratio, and shows that the calculated temperatures are very close to the simulation values, giving agreement to within 5 - 10%. Intriguingly most of the difference between the two results seems to be due to a constant off-set of about 0.2 - 0.5 eV between the simulation and calculation rather than random errors. Temperature as a function of voltage plotted in 3.10 (b) shows a similar agreement, with both simulation and calculated results showing the same small difference.

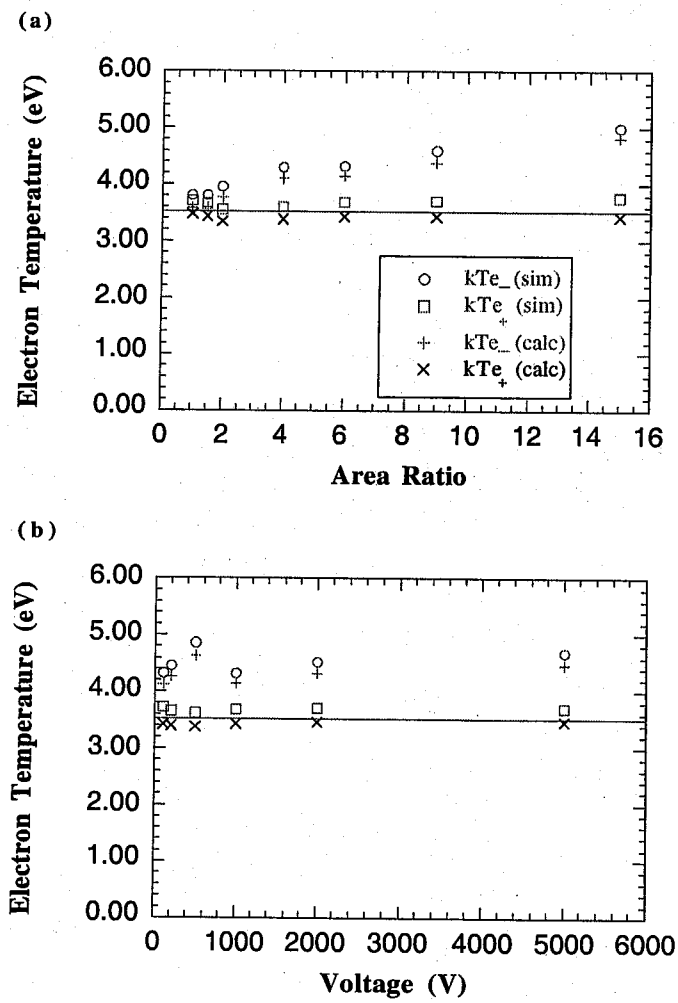

Figure 3.10 The electron temperature for negative, kTe_-, and positive, kTe_+, bulk regions, with simulation results plotted in comparison to calculations from equation (3.49). The solid line is the planar electron temperature, 3.5 eV. Temperatures plotted as functions of **(a)** area ratio **(b)** voltage

One of the difficulties in comparing simulation and calculated values is due to the fact that the *average* temperature is not actually a well defined concept. Equation (3.49) is derived assuming the idealised case in which the two bulk regions have two separate constant temperatures. As mentioned previously, this is not the true situation – in reality the temperature increases from the centre position, r_o, to the sheath edges. The gradient is fairly flat for the positive region of the plasma, and relatively steep for the negative region although in both cases the actual dependency is a function of all the plasma parameters. The "average" value from the simulation is actually obtained by fitting results numerically calculated from equation (3.40), to the potential distribution found from the simulation. The electron temperature is chosen so that the distribution has a good fit at the sheath edges. As the temperature increases toward the sheath edges this method tends to fit the high end of the temperature gradient and thus results in higher average temperatures being accredited to the simulation. Results from the simulation also show that the temperature gradients increase with gas pressure, and so it is harder to find a good "average" temperature at higher pressures (> 50 mTorr).

This method also turns out to be extremely sensitive to the mid-position r_o – if r_o is moved closer to one electrode then the potential gradient will be steeper (to drop the same potential over a shorter region) and so a higher electron temperature will be required to give a good fit to the potential at the sheath edge. This further complicates matters since it is often difficult to determine the exact position of r_o, as is discussed in the next section.

3.2.5 *Mid-position*

The relationship between the mid-position, r_o, and the electrode area ratio α, applied voltage V_{rf}, pressure p and applied frequency f_{rf} has proved difficult to quantify precisely. Partly this is due to the nature of the potential distribution – for many conditions, typically low voltages and area ratios, the bulk potentials are very flat in the centre and so r_o is indeterminate over a range over 2 - 3 cm. This in turn affects the determination of the average bulk temperature, as mentioned in the previous section. For all of the applied parameters r_o is fairly close (within a few centimetres) to the geometric centre of the plasma and so it is, to a first approximation, a function of the electrode radii. Figure 3.11 (a) shows r_o plotted in comparison with $r_{centre} = \frac{1}{2}(r_a + r_b)$ as a function of area ratio. At small area ratios the agreement between the two results is good but at high area ratios r_o is consistently less than r_{centre}. The same effect occurs for high pressures as shown in 3.11(b).

This is due to the non-Maxwellian behaviour of the electrons. Looking at Figure

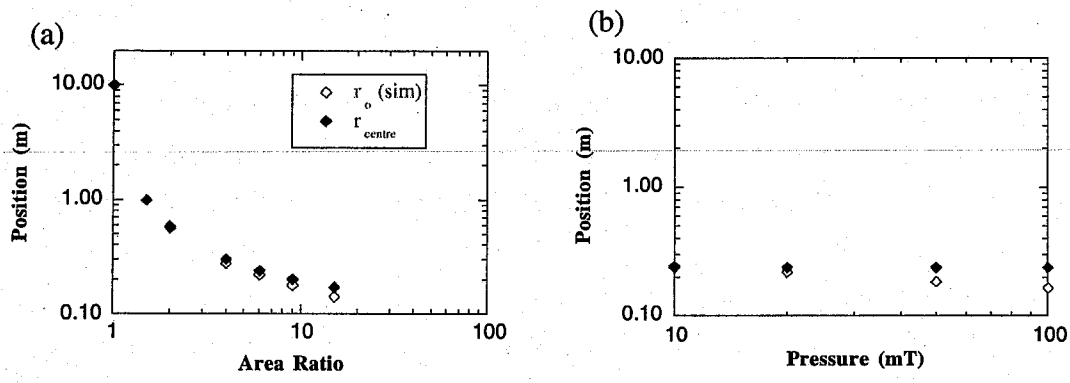

Figure 3.11 The position of peak voltage, r_o, plotted in comparison to the central radius, r_{centre}, as a function of **(a)** area ratio and **(b)** pressure

3.9 it can be seen that the average electron energy is much higher in the region of the live sheath edge. As mentioned in Section (3.2.4) this results in enhanced ionisation in the negative half of the plasma, and so to balance the ion currents to each electrode the volume in which ionisation can take place in the negative region must decrease, hence r_o moves closer to the live electrode. This effect is more noticeable at high area ratios and high pressures, since the temperature gradients are much larger in these cases. In order to determine reasonable values for r_o an iterative technique to fit both electron temperature and r_o must be used. This is outlined in the next section.

3.2.6 Fitting the potential distribution

Having obtained equations for the potential at the sheath edge, the electron temperature and an approximation for the mid-position, the potential distribution in the bulk can now be determined as a function of the system parameters. However to solve for the potential distribution both the electron temperature and the sheath-edge potential have to be known concurrently since they depend on each other. To solve the equations simultaneously an iterative technique is used. Starting with an initial electron temperature of 3.5 eV (the planar temperature), η_s can be calculated from equation (3.44), and then used in (3.40) to determine the bulk widths. Then the electron temperature can be recalculated from (3.49). Determining the sheath widths from another source (say from the simulation, or using the sheath equation (3.28)) then a new value for mid-position r_o can be calculated from the sheath and bulk widths (i.e., $r_o = r_a + s_a + x_-$ or $r_o = r_b - s_b - x_+$). This process is continued until $kT_{e\pm}$, $\eta_{s\pm}$, $x_{s\pm}$ and r_o reach steady-state values. For relatively flat potentials in the bulk and small electron temperature gradients, this process

only requires a few iterations. However, for large temperature gradients it can take a long time to converge to a solution, and in a few cases it will not converge at all unless the parameters are initialised with specifically chosen starting values.

In the following three figures the potential distributions are plotted together with the results from the simulation. The calculated normalised potentials are converted back to volts using the appropriate electron temperatures and are plotted relative to the peak potential determined from the simulation. Figure 3.12 shows the fits for three different area ratios: (a) $\alpha = 1$, (b) $\alpha = 6$ and (c) $\alpha = 15$. It can be seen that the qualitative agreement between simulation and calculated results is very good. The calculated results have the correct slope of the potential gradient for both regions, with higher temperatures in the negative region of the bulk. There is good agreement between simulated and calculated values of r_o.and the potentials at the sheath edges. Note that r_o moves toward the live electrode and kT_e- increases with increasing area ratio. However a detailed look at the potential fits, even at $\alpha = 1$, shows there is a slight discrepancy in the middle of the fit between r_o and the sheath edge. This comes about from using an average temperature rather than a temperature gradient in the bulk calculation. The potentials are effectively fixed at the sheath edges and at r_o, so differences in the fitted and simulated potentials between r_s and r_o are due to the temperature gradient in this region. With higher area ratios, which have steeper potential gradients, the mismatch in the fit is more noticeable.

In Figure 3.13 the potential distribution is plotted for three voltages (a) 100 V (b) 500 V and (c) 5000 V for area ratio, $\alpha = 6$. Much of what has been said for the potential distribution as a function of area ratio is also applicable here – for low voltages, where the temperature gradients are small, the fits are better than at high voltages. Discrepancies between the simulation and the analytic model are of the order of a few volts and overall the qualitative fit is very good.

Figure 3.14 shows the fits for pressures (a) 10 mTorr (b) 50 mTorr and (c) 100 mTorr. The fit to the simulation is very good at 10 mTorr, but decreases at higher pressures, especially in the positive bulk region. This is due to increasing temperature gradients in the system, for which the approximation of using an average electron temperature breaks down. 100 mTorr probably represents the limit of validity of this derivation of the bulk potentials. To derive potentials at higher pressures it would be necessary to include temperature gradients in Poisson's equation, which would then have to be solved numerically.

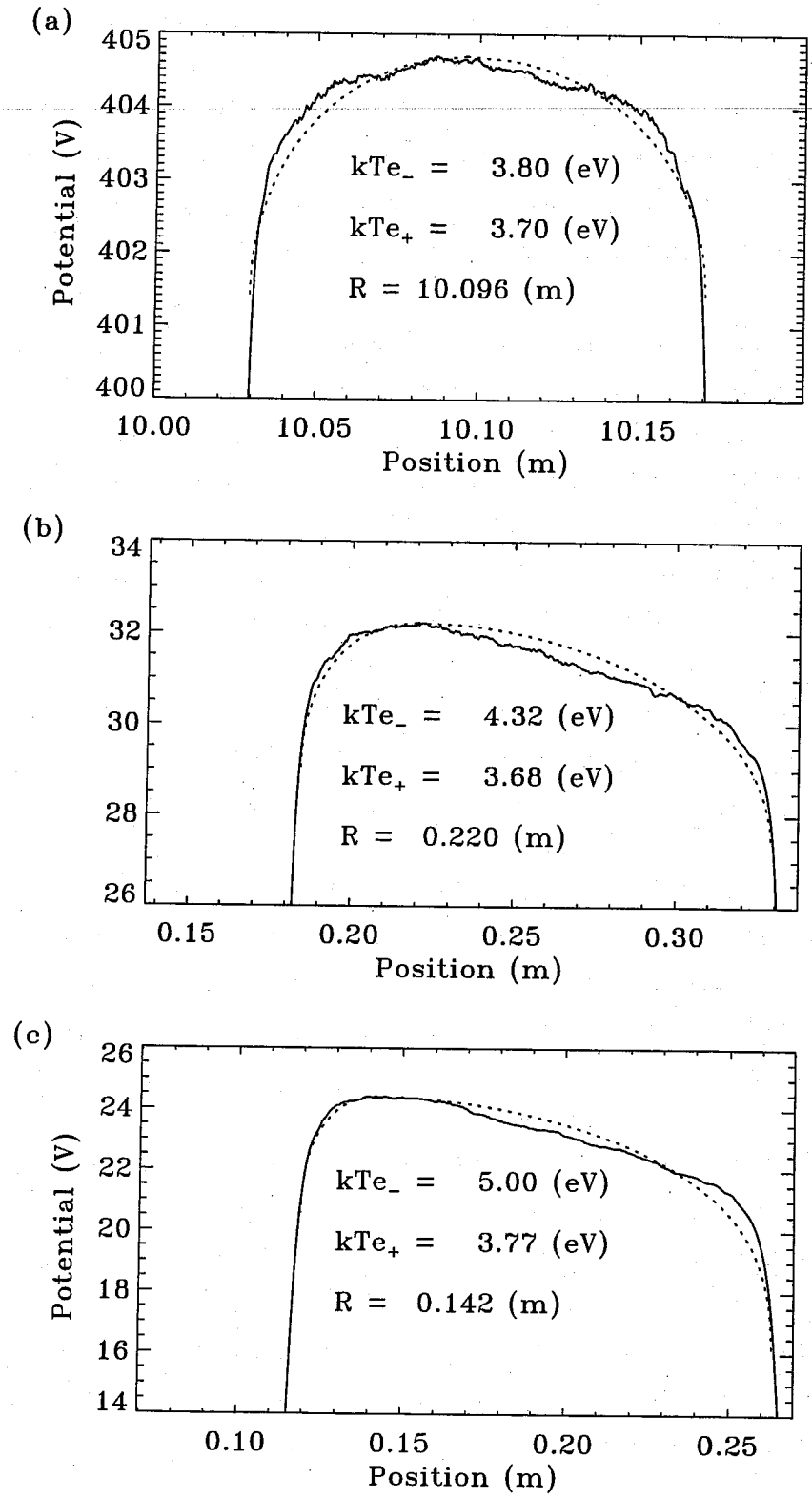

Figure 3.12 Potential distribution in the bulk for various area ratios comparing simulation results (solid line) with analytic solutions (dotted line). Electron temperatures and mid-position from the calculations are shown on the plots. Area ratios are: (a) α = 1, (b) α = 6 (c) α = 15

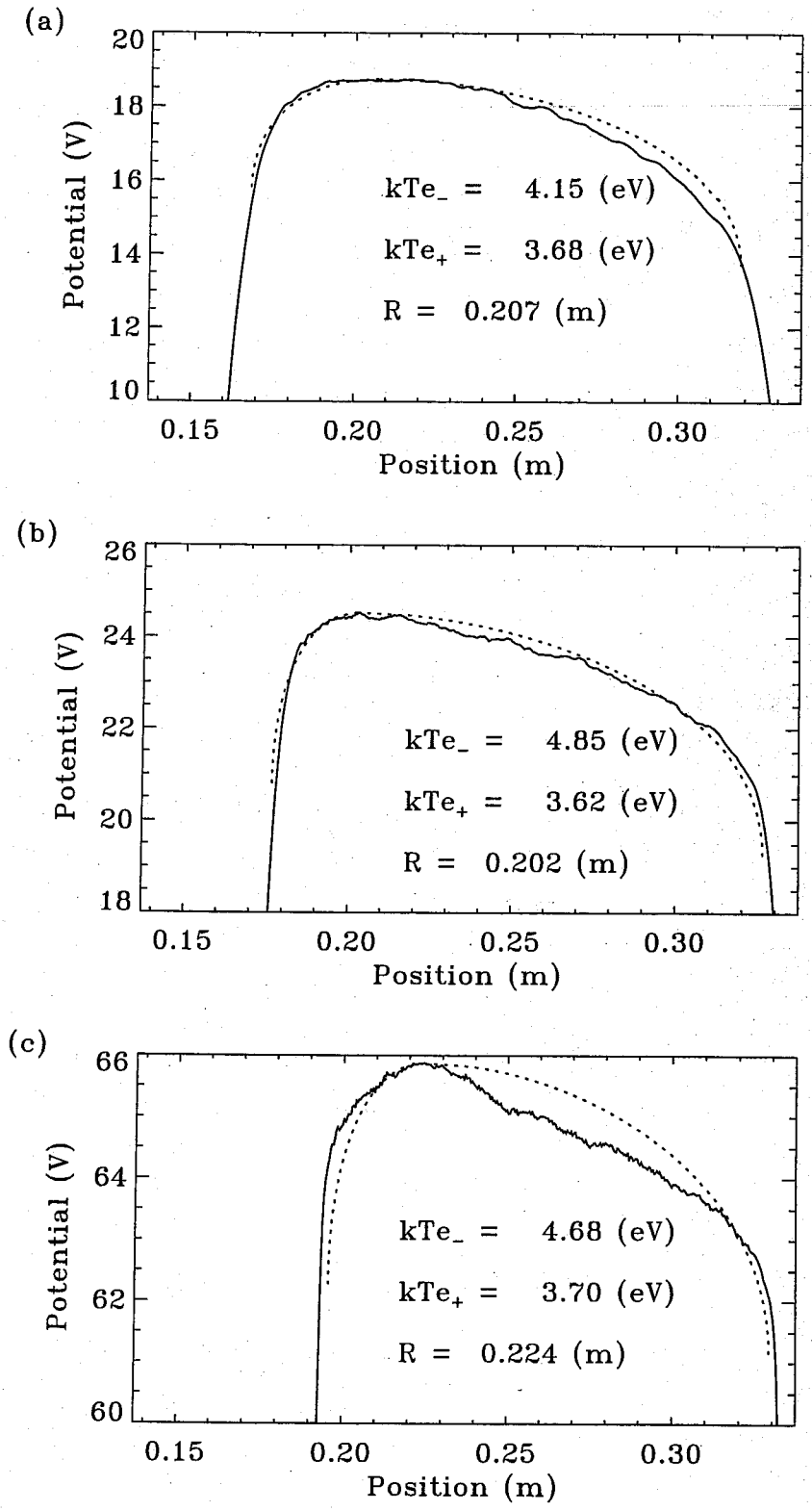

Figure 3.13 Potential distribution in the bulk for different applied voltages comparing simulation results (solid line) and analytic solution (dotted line). Electron temperatures and mid-position from the calculation are shown on the plots. Voltages are (a) V_{rf} = 100V, (b) V_{rf} = 500V (c) V_{rf} = 5kV

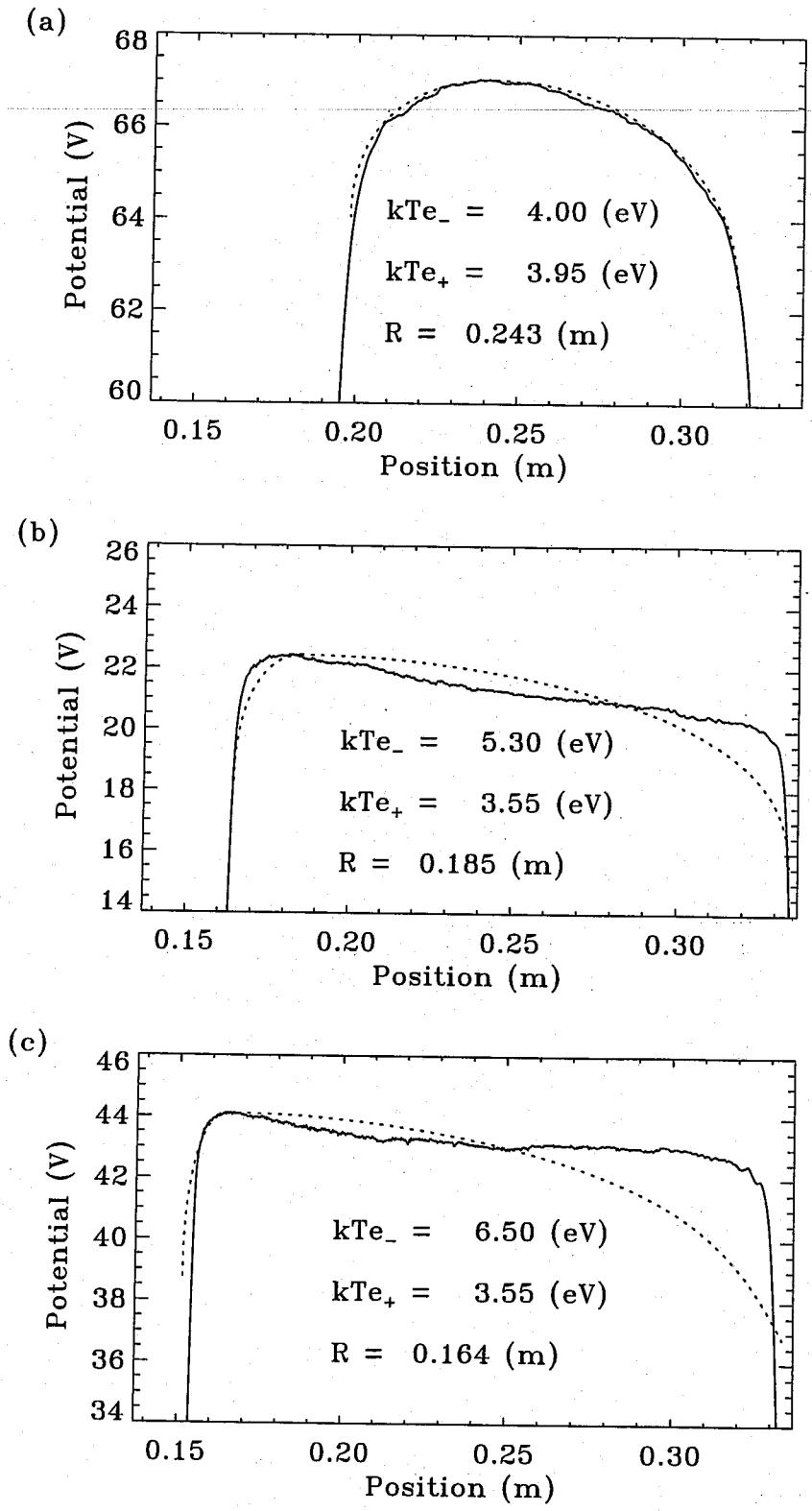

Figure 3.14 Potential distribution in the bulk for different gas pressures comparing simulation results (solid line) and analytic solution (dotted line). Electron temperatures and mid–position from the calculations are shown on plots. Pressures are (a) pres = 10mT (b) pres = 50mT (c) pres = 100mT

3.2.7 *Fitting to the bulk density*

Assuming a Maxwellian distribution for the electrons in the bulk, the density distribution can be described by $n(x) = n_o e^{-\eta}$ (equation (3.29)). However it is sometimes more convenient to have the density as a function of position rather than potential (as when deriving the electron temperature in Section 3.2.4 and the bulk ion current in Section 3.2.6) and from equation (3.30) it would appear that the density distribution should be proportional to $(x/x_s)^2$. Looking at the simulation results the density is indeed found to have a parabolic dependance on position and can be empirically fitted with a function of the form

$$n(x) = n_o\left[1-(1-\zeta)(x/x_s)^2\right], \qquad (3.50)$$

where $\zeta = e^{-\eta_s}$, so that at $x = x_s$ the boundary condition $n_s = n_o e^{-\eta_s}$ is obtained.

The fit for an electrode area ratio of 6 is shown in Figure (3.15), which compares the simulation density distribution with the fit taken from equation (3.50), and with the Maxwellian density distribution. The parabolic fit is very good except close to the grounded sheath edge where the potential gradient is smaller; interestingly (3.50) provides a better fit in the negative region than the Maxwellian density equation. Overall

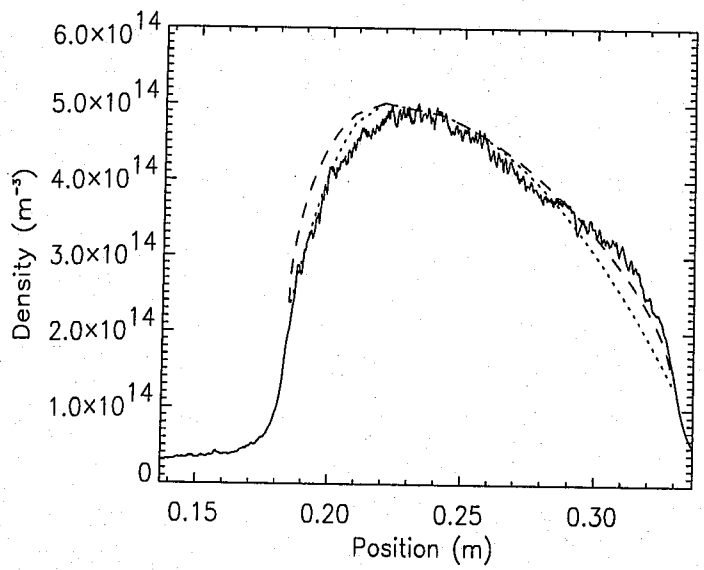

Figure 3.15 Density in the bulk showing simulation results (solid line) fitted with parabolic equation (3.50) (dotted line) and the maxwellian density distribution (dashed line), for $\alpha = 6$

(3.50) fits the simulation results to within about 10% for all area ratios and voltages, but doesn't fit quite as well to the high end of the pressure scale due to the steep gradients in the electron temperature (neither Maxwellian nor parabolic fits work well in that case).

3.2.8 *Ion Current Calculation*

One of the main plasma parameters to be determined from the bulk calculations is the ion current at the sheath edge. This can be then used in the sheath equation to determine the average potential across the sheath as a function of the maximum sheath width. As with the electron temperature, the ion current is determined by balancing the creation rate of ions within the bulk with the loss rate to the walls (otherwise the bulk density would increase and the system would not be at steady state). Hence the ion current is essentially a function of the ionisation rate and the plasma density. Ions created in the bulk must be lost to their local electrode, as the ion drift velocity is determined by the average local potentials which monotonically decrease from r_o to the sheath edges. Therefore the total current at each sheath edge is determined by a volume integral over the total number of ionising collisions in the corresponding bulk region, i.e.,

$$i_{\pm}(x) = \int_0^x e\, n_i(z)\, \nu_I(z) 4\pi (r_o \pm z)^2 dz\,. \qquad (3.51)$$

This equation can be simplified by assuming that ν_I is independent of position – i.e., the temperature gradients are assumed to be small, so that the electron temperature is constant in each half of the bulk . Equation (3.50) is used to fit the spatial variation of the density, so that the integral in (3.51) depends only on x (the Maxwellian density, equation (3.29), is not used since it is dependent on the bulk potential which would make (3.51) much more complex to solve). The current at the sheath edge, i_s, is then given by

$$i_{s\pm} = 4\pi e\, \nu_I n_o x_{s\pm}\left(0.808 r_o^{\,2} \pm 0.712 r_o x_{s\pm} + 0.218 x_{s\pm}^{\,2}\right). \qquad (3.52)$$

The accuracy of the fitting is shown in Figure (3.4) where the ion current determined from (3.52) is plotted together with results from the simulation and equation (3.28).

The ion current to each electrode depends on the volume ionisation rate in the region of the bulk close to it. This in turn depends on the density in the bulk, the electron temperature, the potential distribution in the bulk and so on. The ion currents calculated from equation (3.52) are found to be particularly sensitive to the position of r_o, since ions created at radii $< r_o$ will go to the live electrode, while those at radii $> r_o$ will go to

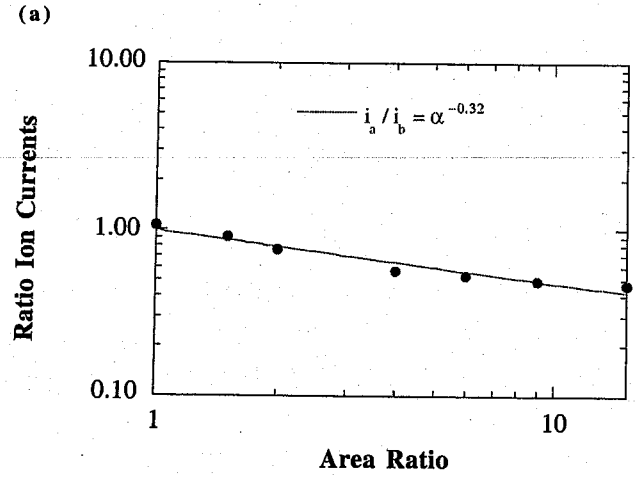

Figure 3.16 Ratio of live to grounded ion currents as a function of area ratio. The dots represent results from the simulation, and the line was fitted using least squares methods.

the grounded electrode. The ratio of the ion currents at the electrodes is found to be relatively independent of applied voltage and pressure, and is mainly determined by area ratio and frequency. The dependence on area ratio is shown in Figure 3.16.

With increasing area ratio r_o moves closer to r_a, since the average potential peaks closer to the inner electrode at higher area ratios and has a long tail-off toward the outer electrode. This can be seen in the bulk potential plots in Figure 3.12. This causes a decrease in current to the inner electrode relative to the current at the outer electrode, due to the decrease in the bulk region where ions can be created. However at the same time the average electron energy close to the live electrode is increasing with area ratio (see Figure 3.9), and so the ratio of the ion currents represents a balance between these two processes, leading to the relationship plotted in Figure 3.16

3.2.9 Comparison with other numerical models

Bissell, Johnson and Stangeby (1989) published a review of two kinetic and two fluid models of a one-dimensional collisionless bulk plasma. These models were used to examine the steady-state flow of plasma to a boundary, with particular application to fusion plasmas. Since in fusion plasmas the ionisation fraction is typically large and the ion temperatures are also large this means that some of the assumptions used in the models will not be applicable to the PIC results. They do, however, include some results

for zero ion temperature, and these can be compared to results from the simulation and model derived in this chapter.

The kinetic models (Bissell and Johnson (1987) and Emmert *et al* (1980)) are also based on the derivation by Tonks and Langmuir (1929), the main difference in the models being that ions are no longer assumed to be created cold (since in fusion plasmas the background neutrals have temperatures of the order of T_e) and so a source function which models the ion temperature is included. This complicates the equations, requiring the models to be solved numerically rather than analytically. The two kinetic models are differentiated by different source functions. Since ions in processing plasma *are* created cold the limit as $kT_i \rightarrow 0$ is used, for which both models give the same answer.

The two fluid cases are for an isothermal and an adiabatic model. The isothermal model assumes that the ion pressure is isotropic and the ion temperature is constant, i.e., $p_{||} = p_{\perp} = nkT_i$, while the adiabatic model has different parallel and perpendicular temperatures. The fluid models were made to be collisionless by leaving out the explicit collisional terms in the momentum and energy equations, although this does leave implicit ion-ion collisions in the adiabatic model due to the closure condition used.

	Kinetic	**Adiabatic**	**Isothermal**	**Analytic Model**	**PIC Simulation**
η_s	0.854	0.783	0.693	0.857	0.88
n_s/n_o	0.426	0.457	0.5	0.424	0.35
$<v>/u_b$	1.144	1.068	1.0	1.177	1.384

Table 3.1 Values of normalised potential, η_s, density ratio n_s/n_o, and ion velocity $<v>/u_b$ at the sheath edge are listed for the kinetic, adiabatic and isothermal models from Bissell *et al* in comparison to the analytic model presented in this chapter and the simulation results.

Results from the $T_i = 0$ case for the different models in Bissel *et al* are compared with simulation and model results with an area ratio of 1 in Table 3.1. The comparison is made between the normalised potential at the sheath edge, η_s, the density at the sheath edge normalised to the peak density, n_s/n_o, and the average velocity at the sheath edge normalised by the ion sound speed, $<v>/u_b$. Obviously results from the kinematic model used by Bissell *et al* (1989) and the model derived in this thesis are very similar, which is to be expected since at $T_i = 0$ they are essentially the same model (although the model

from Bissell *et al* is solved numerically rather than analytically). The agreement with the adiabatic model is extremely good, while the isothermal model follows the general trend correctly. Overall the agreement between the models and the simulation is to within 20%.

3.3 Sheath scaling laws

The ion current calculated in section 3.2.7 can be used in the sheath equation (3.28), to determine the sheath voltage and width. However, further equations relating the sheath widths and average sheath potentials must be obtained to act as closure conditions for the model, and thus fully quantify the plasma. Once these equations have been found the sheath and bulk equations can be solved concurrently to determine the average potential and density distributions, the ion currents at the electrodes, the electron temperature(s), and the ion energies at the electrodes.

In Section 3.3.1 the relationship between the sheath width and average voltage is determined from the ion power which is derived from the total applied power to the simulations. In Section 3.3.2 the voltage division is determined from the sheath capacitance relating the sheath width to the rf voltage across the sheaths. Finally in Section 3.3.3 an equation for the peak density is derived empirically from the simulations.

3.3.1 Capacitive voltage division between the sheaths

In order to determine the average ion energies at the electrodes it is necessary to determine how the voltage is distributed across the plasma, since voltage division between the sheaths is complex in the asymmetric system and depends on all the applied parameters. Using a simple equivalent circuit model of the plasma, at frequencies of around 10 MHz and pressures less than 1 Torr the sheath impedance is predominantly capacitive. Therefore treating the sheaths as two capacitors in series the voltage across each sheath can be determined using capacitive division, where the individual sheath capacitances are calculated using $CV = Q$. Due to the moving electron sheath the charge in the sheath is constantly changing during the cycle, and so this equation must be differentiated with respect to time. Assuming that the sheath capacitance is independent of the rf period, the total rf current is a function of the changing voltage only:

$$C\frac{\partial V(t)}{\partial t} = \frac{\partial Q}{\partial t} = I(t), \tag{3.53}$$

Note that this equation uses the total discharge current, I. In the sheath I is mainly in the form of a displacement current, except for the brief period each cycle when the sheath collapses and electrons can enter. The rf current is approximately sinusoidal in shape (see Figure 4.13) and has the same period as the applied voltage with a phase difference of ϕ. Hence the rf current has the form $I(t) = I_{rf}\sin(\omega t + \phi)$; substituting this back into equation (3.53) it is found that

$$CV_{rf}\frac{\partial \sin \omega t}{\partial t} = I_{rf}\frac{\partial \sin(\omega t + \phi)}{\partial t},$$

$$C = \frac{I_{rf}}{\omega V_{rf}}(\tan \omega t \cos \phi + \sin \phi). \qquad (3.54)$$

where V_{rf} is the amplitude of the applied voltage. For a purely capacitive system (i.e., if sheath impedance purely capacitive and the bulk impedance negligible) then the phase difference between the current and voltage, ϕ, would be equal to 90° and (3.54) would simplify to $C = I_{rf}/\omega V_{rf}$. However results from the simulation indicate that this is not the case, although it is often assumed so in deriving the electrical response of the sheath. Instead the phase difference is found to have an average value of $\phi = 73°$, essentially independent of the input parameters. The high value of ϕ indicates the system is predominantly capacitive as expected, although in Chapter 4 it is shown that both the sheath and bulk also have a resistive component. Experimental measurements by Bletzinger and Flemming (1987) in argon show that the phase shift between current and voltage is relatively independent of pressure in the range 0.1 - 1 Torr, varying slowly between 80 to 70° (for pressures > 2 Torr ϕ drops to ~40°). Substituting for ϕ in equation (3.54) gives

$$C = \frac{I_{rf}}{\omega V_{rf}}(0.29\tan \omega t + 0.96). \qquad (3.54)$$

Hence C is not independent of time, as previously assumed. Simulation results show that the capacitance is very close to constant for most of the cycle, but twice per cycle at $\omega t = \pi/4$ and $\omega t = 3\pi/4$, for periods of about 150 ns the capacitance suddenly becomes very large. These times correspond to the periods of sheath collapse at the live and grounded electrodes, at which time the sheath width effectively goes to zero and so the capacitance becomes infinite.

A geometric value for the sheath capacitance can also be determined by relating the sheath to a real capacitor of the same dimensions. The boundaries of the sheath are chosen to be the electrode on one side and the position of maximum sheath width on the

other (to include the entire exclusion zone for the electrons). Hence the capacitance in spherical coordinates can be calculated using

$$C = \frac{4\pi\varepsilon_o r_{elec} r_s}{s}, \tag{3.56}$$

where r_{elec} is the electrode radius, r_s the radius of the maximum sheath extension and s is the maximum sheath width ($= r_s - r_{elec}$). Equating equations (3.55) and (3.56) relates the sheath width to the rf voltage across each sheath, that is

$$C_a = \frac{4\pi r_a (r_a + s_a)}{s_a} = \kappa_a \frac{I_{rf}}{\omega |V_a|}, \tag{3.57(a)}$$

$$C_b = \frac{4\pi r_b (r_b - s_b)}{s_b} = \kappa_b \frac{I_{rf}}{\omega |V_b|}, \tag{3.57(b)}$$

where r_a and r_b refer to the radii of the powered and grounded electrodes respectively, and $|V_a|$ and $|V_b|$ to the amplitude of the sheath voltage at each electrode (the sheath voltage is assumed to vary sinusoidally over the rf cycle). This assumes that in equation (3.54) $(0.29\tan\omega t + 0.96) \approx \kappa = \text{constant}$ for the whole cycle and neglects the period in which the capacitance becomes large, since this relates to only 1.5% of the cycle. Averaging simulation results over area ratio, voltage, frequency and pressure the two constants are found to be $\kappa_a = 0.765$, and $\kappa_b = 0.59$.

Using capacitive voltage division the ratio of the sheath amplitudes can be determined from equations 3.57(a) and (b):

$$\frac{|V_a|}{|V_b|} = 1.297\alpha \frac{s_a}{s_b}\left(\frac{1 - s_b/r_b}{1 + s_a/r_a}\right). \tag{3.58}$$

The results from (3.58) are plotted in Figure 3.17, in comparison with results from the simulation as a function of area ratio. The correlation is very good except at area ratio 1, where the method of averaging breaks down due to the large areas of the sheaths (10 m radii electrodes are used in this case). In the case where $s_b << r_b$ and $s_a << r_a$ (i.e., at large electrode radii, so small area ratios) from equation (3.56) $|V_a|/|V_b| \propto \alpha \frac{s_a}{s_b}$. In Section 4.1 it is shown that the ratio of the sheath widths (neglecting density effects) is also approximately proportional to the area ratio, and hence the voltage ratio should roughly depend on the area ratio squared. This proportionality is shown in Figure 3.17, and while the approximation is fairly rough it is seen to follow the correct trend of the data. The middle range values are larger than α^2 due to neglecting the effect of the sheath

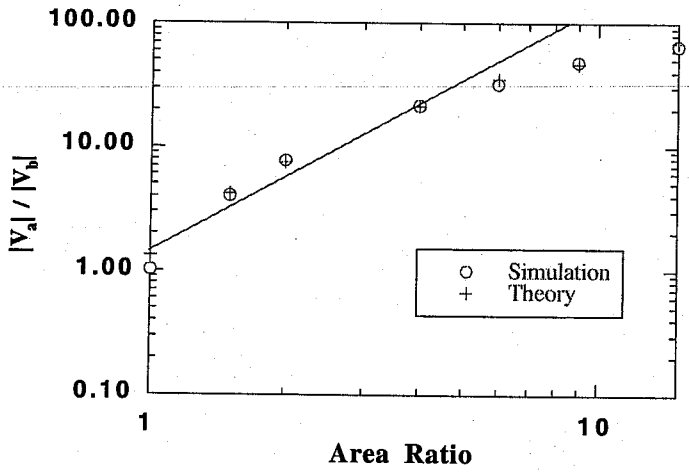

Figure 3.17 Ratio of the sheath voltage amplitudes from the simulation (circles) plotted in comparison with results from equation (3.58) (crosses). The solid line shows proportionality to α^2

density, while at high area ratios the voltage ratio saturates, as the sheath width approaches the magnitude of the electrode radius.

Equation (3.58) relates the *amplitude* of the rf voltage across each sheath, but does not determine the relationship between the time-averaged sheath voltages. It is generally assumed that the rf and dc components of the sheath voltage are linearly related provided the rf voltage is greater than 20V for pressures of around 10 - 100 mTorr (Godyak *et al*(1991b)). The simulation results for the average sheath voltage as a function of the rf sheath voltage for the live and grounded electrode are plotted in Figures 3.18(a) and (b). Note that the potentials plotted here are measured between the position of peak potential (at r_o) and the electrode rather than the sheath edge and the electrode, since the former is easier to measure and there is only a few volts difference between the two methods. The linear relationship between rf and dc (average) voltages holds well for both electrodes, except at very low voltages at the grounded electrode. This is due to the development of a positive dc offset on the plasma potential at low voltages, as described in Section 4.1

To understand why the live sheath voltage is so much greater than the grounded sheath voltage in asymmetric geometries (at high area ratios it can be 70 times larger) consider first of all a symmetric system, which has equal sheath voltages and widths. If the area of one electrode is increased then it follows from $C \propto A/l$ that the sheath at the larger electrode will have a larger capacitance and hence a smaller proportion of the voltage will be dropped across it. Consequently, for the system geometry described in

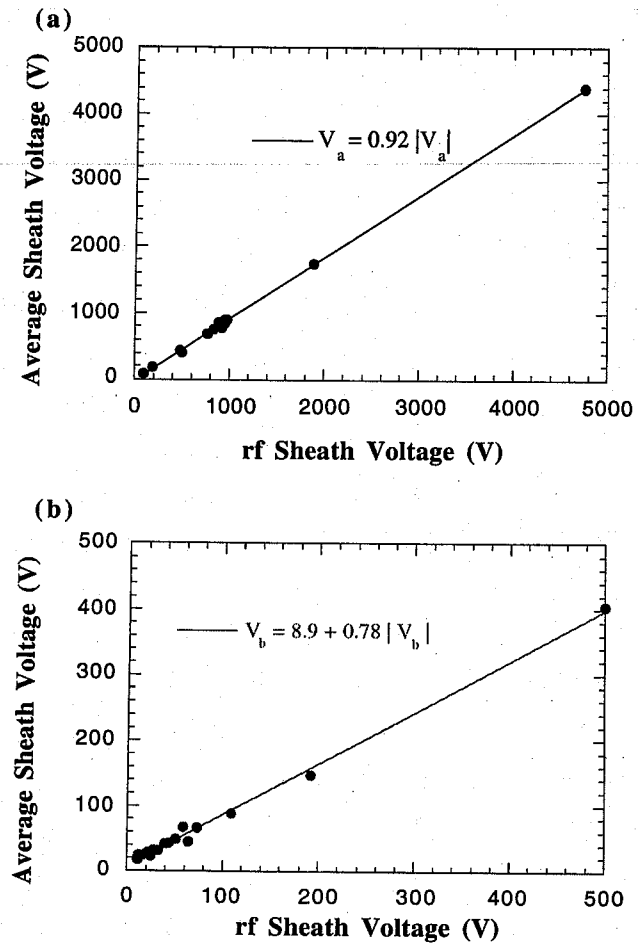

Figure 3.18 The average sheath voltage plotted against the rf sheath voltage for **(a)** live and **(b)** grounded electrodes

this thesis, the proportion of the applied potential that is dropped across the live electrode sheath will be larger than that at the grounded sheath, purely from consideration of capacitive division. Thus, as the voltage ratio increases, from equation (3.58) the ratio of the live to grounded sheath widths, s_a/s_b, must also increase. Now from Section 3.2.3 the total bulk width is constant (with respect to area ratio) and hence the sum of the two sheath widths must also be constant. Therefore as the live sheath width increases the grounded sheath must decrease until an equilibrium between the potentials and the sheath widths is reached. These values are not easily calculated since as the sheath width changes so also does the sheath capacitance, and therefore the sheath voltage.

Now consider the *average* (or dc) voltage across each sheath: this must be at least of sufficient magnitude to contain the electrons and maintain the plasma, and its lower limit can therefore be assumed to be the floating potential. The floating potential V_f is simply the potential of a plasma in an earthed container and it is found to be proportional to the electron temperature (see Vender (1990), pg 55): for a hydrogen plasma $V_f \sim 4kT_e$.

Assuming a linear relationship between rf and dc voltages (as shown in Figure 3.18), the floating potential in effect places a lower limit on the rf voltage. As the area ratio is increased the ratio of the rf sheath voltages must also increase (since $|V_a|$ increases and $|V_b|$ decreases), but from the above argument it is expected that at very large area ratios the rf voltage ratio must reach a steady-state value since the sum of the sheath voltages cannot exceed the applied voltage and the rf ground sheath voltage will be limited by the floating potential. This in turn places a restriction on the minimum sheath width at the grounded electrode via the sheath equation (assuming the ion current remains constant, or at least does not increase). Results from the simulation show this saturation in both the voltage and sheath ratios at very large α (see Figures 3.17 and 4.y), but also indicate that the mechanism is more complicated than assumed above, since at high area ratios the plasma potential develops a positive dc offset. This retains the electrons even as the rf voltage across the grounded sheath continues to decrease, by allowing the rf voltage amplitude across the sheath to be smaller than the average voltage (i.e., there is a breakdown in the linear proportionality between rf and dc voltages at very low voltages). However, even with this effect the ground voltage cannot keep decreasing and at very large area ratios the ratio of the rf sheath voltages saturates as shown.

At the live electrode a large negative dc potential is created by charging the circuit capacitor negatively in the first few microseconds of running the plasma. This limits the maximum excursion of the live electrode voltage to approximately the magnitude of the bulk plasma potential, and thus reduces the number of escaping electrons so that electron and ion losses balance over an rf cycle. In actual fact simulation results show that, contrary to popular belief, the electrode potential can transiently reach values which are much larger than the bulk potential (see Section 4.1 for a detailed results). This is because under certain conditions the fields at the powered electrode are changing so rapidly (much faster than the plasma frequency) that inertia prevents electrons responding instantaneously to the fields. Therefore a positive sheath potential develops in order to accelerate the electrons out of the plasma and thus balance ion and electron currents during the cycle. This gives the electrons a beam-like velocity distribution, which has previously been observed in planar simulations (Vender and Boswell (1992)). The effect is magnified when the sheath width and potential are large and so is particularly noticeable at large area ratios and voltages. The ions are unaffected by the positive excursion of the sheath potential since they only react to the cycle-averaged fields due to their large mass.

3.3.2 Ion Power Calculations

An alternative method of determining the average sheath voltage, especially when the voltage dropped across the sheath is small and the linear relationship between rf and dc no longer applies, is to use the ion power. Power derivations are discussed in detail in Chapter 4 and here it is sufficient to say that the power dissipated by the ions at each electrode is related to the ion current at the electrode and the sheath potential, by:

$$P_{ion} = i_a V_a + i_b V_b. \tag{3.59}$$

For $\alpha = 1$ the currents and voltages at each electrode are equal and so (3.59) becomes $P_{ion} = 2i_a V_a$; and for $\alpha \geq 2$ the ion power at the live electrode is approximately an order of magnitude greater than power dissipated at the grounded electrode, therefore (3.59) can be effectively represented by $P_{ion} = i_a V_a$. From (4.27) the relationship between the total power dissipated by the plasma and the ion power is given by $P_{ion} = P_{tot}/2$, so the average live sheath potential can be related to the total power and the ion current by

$$V_a = 0.99 \frac{P_{tot}}{i_a} \qquad \text{for } \alpha = 1$$
$$V_a = 0.495 \frac{P_{tot}}{i_a} \qquad \text{for } \alpha \geq 2 \tag{3.60}$$

Note that this method is only useful for finding the average potential at the live electrode, except for $\alpha = 1$ where both live and ground potentials are equal.

3.3.3 Peak Density Measurement

In order to calculate the ion current from equation (3.52) it is first necessary to determine a value for the peak density in the plasma. The steady-state plasma density is a result of the balance between production rate through electron ionisation collisions, and the loss rate of particles to the walls. Consequently the density is expected to depend in some complex fashion on the deposition of power into the electrons, ionisation cross-section, neutral gas pressure, system volume and ion currents to the walls. Simulation results show that the power per charged species $P_{tot} / N_{\pm}$, dissipated by the plasma is a function only of the applied voltage, and is therefore independent of the other plasma parameters. The dependence on voltage is shown in Figure 3.19. This plot shows that the data appears to have a different dependance on V_{rf} for low and high voltages – for $V_{rf} < 500$ V $P_{tot} / N \propto V_{rf}^{0.5}$, while for $V_{rf} > 500$ V $P_{tot} / N \propto V_{rf}$. Fitting to the simulation results gives the equations:

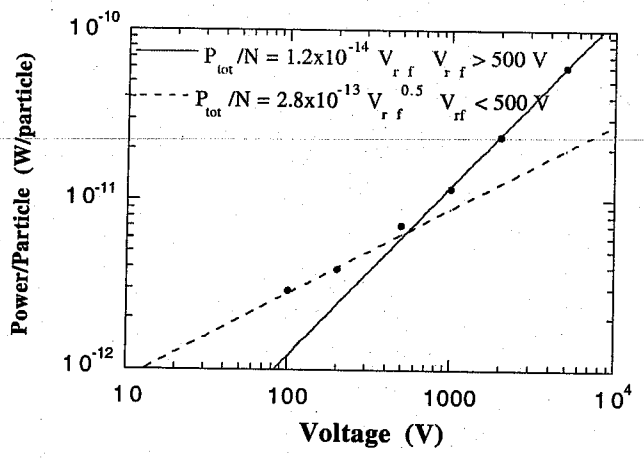

Figure 3.19 The applied power per plasma species as a function of the applied voltage.

$$\frac{P_{tot}}{N_{\pm}} = 2.8\times10^{-13} V_{rf}^{1/2} \quad V_{rf} < 500\ V, \tag{3.61(a)}$$

$$\frac{P_{tot}}{N_{\pm}} = 1.2\times10^{-14} V_{rf} \quad V_{rf} > 500\ V, \tag{3.61(b)}$$

where $N_{\pm}$ is the number of ions/electrons in the plasma.

The difference at low and high voltages could indicate different mechanisms by which power is transferred to the particles, or possibly just a lower limit on the power required to balance loss rates and maintain the plasma. Experimental results in argon (Godyak*et al* (1991b)) show a similar change in the power/voltage behaviour with $P_{tot} \propto V_{rf}$ at low currents and $P_{tot} \propto V_{rf}^2$ at high currents.

Equation (3.61) therefore relates the input power and the applied voltage, known parameters of the plasma, to the total number of particles in the plasma. This can then be related to the average plasma density by dividing through by the system volume. The average plasma density is found by integrating over equation (3.50). The equation can be simplified by assuming the system is relatively symmetric, then from equation (3.43) $(1 - \zeta) = 1 - e^{-\eta_p} = 0.776$, giving

$$n_{avg} = \frac{n_o}{L/2}\int_0^{x_s}\left[1-(1-\zeta)\left(\frac{x}{x_s}\right)^2\right]dx$$

$$= \frac{n_o}{L/2}0.808x_s, \tag{3.62}$$

where L is the system length. Assuming $L/2 \approx x_s$, then re-arranging (3.62) gives

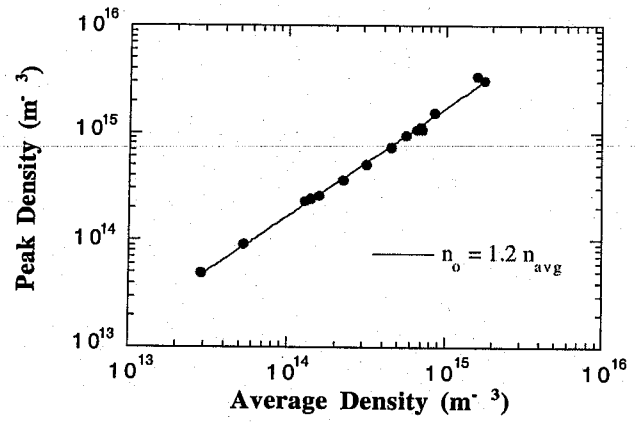

Figure 3.20 The peak density plotted as a function of the average density, showing simulation results (dots), and fitted equation (line).

$n_O = 1.24\ n_{avg}$. Plotting the peak density as a function of the average density in Figure 3.20, least-squares fitting gives the relationship between the two densities to be $n_O = 1.2\ n_{avg}$ over the entire parameter range, in extremely close agreement with the previous determination. Thus the average power dissipated by the plasma, the applied voltage and the system volume can be used to determine the peak density, giving values which are within about 20% of the simulation results.

3.3.4 Bulk and sheath calculations combined

Using the above derivations it is possible to iteratively solve both sheath and bulk equations. Using as given input parameters the electrode radii, gas pressure, input power, and the source voltage and frequency predictions for the potential and density distributions in the bulk, electron temperature, plasma density, ion currents to the electrode, sheath widths and dc and rf sheath potentials can be obtained. As for the bulk case a set of starting conditions are guessed at and the equations are iterated until the solutions reach a steady-state. Note that the system is complex so it is sometimes difficult to obtain convergence, and both convergence and accuracy can depend on the sequence in which the equations are applied. Good results can be obtained for most of the range of area ratios and voltages at low pressures ($\leq$ 50 mTorr). The results for the standard case – $\alpha = 6$, $V_{rf} = 1000$V, $p = 20$ mTorr and $f_{rf} = 10$ MHz – are compared to the simulation results in Table 3.2.

	Simulation	Model	% difference
n_o (m^{-3})	5.0 x 10^{14}	4.4 x 10^{14}	-12%
s_a (m)	0.0463	0.05	+8%
s_b (m)	0.0074	0.012	+62%
i_a (A)	0.44	0.36	-18%
i_b (A)	0.83	0.8	-3.6%
rf V_a (V)	932	963	+3.3%
dc V_a (V)	857	854	-0.3%
rf V_b (V)	32	38	+19%
dc V_b (V)	27	38	+41%
η_{s-} (m^{-3})	0.765	0.78	+2.0%
η_{s+} (m^{-3})	1.32	1.32	0%
r_o (m)	0.22	0.22	0%
x_{s-} (m)	0.035	0.0305	-13%
x_{s+} (m)	0.108	0.106	-2%
kT_{e-} (eV)	4.32	4.55	+5%
kT_{e+} (eV)	3.7	3.68	-0.5%

Table 3.2 Comparison between model and simulation for plasma parameters at the conditions $\alpha = 6$, $V_{rf} = 1000$V, $p = 20$ mTorr and $f_{rf} = 10$ MHz. In general agreement over the range of values is extremely good for this set

In general, agreement over the range of values is extremely good for this set of conditions, with, in most cases, the difference between the simulation and the model being less than 10%. The bulk parameters show even greater accuracy. The largest differences appear in the dc voltage at the grounded electrode, dc V_b, and the grounded sheath width, s_b. As previously discussed in Section 3.3.1, the empirical relationship between dc and rf voltages does not hold well at low voltages. The sheath width calculation is dependent on the dc sheath voltage and so is also inaccurate at these values. Furthermore the simulation measurements have large errors at these low values, since noise levels are large relative to the average values presented here. Overall this model works extremely well in predicting the bulk and sheath parameters for rf plasmas at low pressures for a range of applied voltages and area ratios.

3.4 Conclusion

Analytic models of the sheath and bulk are presented here for spherical geometries. Both models consider the time-averaged potential and density distributions and hence are only able to predict events on the ion time scale. The sheath model considers the effect of a finite electron density in the sheath on the total space charge and uses this to derive a sheath law which relates the ion current, sheath width and average potential in asymmetric geometry. Calculations of the ion current using this law are found to compare well to simulation results.

The bulk calculations determine the average potential profile across the plasma, using a kinetic approach, similar to that of Langmuir and Tonks (1929). The model also determines analytic equations for plasma density profiles, ion current and electron temperature. These derivations show reasonable to very good agreement with simulation results. The model is limited to low pressures by the assumption of a constant electron temperature in the plasma, although by modifying this assumption, so that two different temperatures can be used in the positive and negative regions of the plasma, the range of application can be extended.

An analytic derivation of the sheath capacitance is used to determine the ratio of the amplitude of the sheath voltages. Analytic derivations and scaling laws derived from simulation results are used to find the total number of plasma particles produced for a given applied rf voltage and power, which can be used to determine the peak density in the plasma. These expressions are used together with the bulk and sheath equations to create a global model of the entire plasma, in which predictions of plasma parameters such as sheath widths, currents, potential and density distributions, average electron energy etc, can be made when the system geometry, gas pressure and applied source voltage and power is known.

In summary, the model provides some simple analytic expressions which produce results that agree well with the simulation data, provided the limitations of the model are recognised.

Chapter 4

Simulation results in Hydrogen

Parallel plate reactors are often used for reactive ion etching (RIE) processes. The reactor is used to produce a plasma of a molecular gas, such as SF_6 or CH_4, depending on the material to be etched. The gas is dissociated in the plasma to provide reactive neutral species (e.g., F or H) which can chemically react with the substrate to perform the etching, and also provides a source of energetic ions to drive the etching process (the role of the ions is discussed in Section 4.6). RIE is used as part of the production technique for many different micro-technologies, just a few examples include production of trench capacitors; planar, buried or ridge semi-conductor lasers and optical splitters. As microelectronic technologies become increasingly sophisticated more device components are included per circuit, which necessitates making each device smaller and packing them closer together. This requires extremely good control of parameters such as uniformity of the plasma density across the whole wafer; the energy and angular distributions of ions at the substrate surface; and ion and neutral fluxes. To accomplish this it is critical to have a good understanding of the plasma response to a wide range of running conditions.

Recent work suggests that the ion energy distribution at the substrate is critical in determining etching rates in RIE processing of SiO_2 (Perry (1994)) and also influences film properties in deposition processes (Ichiki, Momose and Yoshida (1994)). Fast etching rates are important for economical production of wafers since faster etching gives a faster turn-around on processing time. However conditions which produce fast etching are also conducive to substrate damage and so a balance must be maintained between etching rates and damage. Average plasma potentials determine the average energy of ions at the substrate, but rf effects can lead to ions arriving with much larger or smaller energies. Hence it is extremely important to determine the ion energy distribution function (IEDF) at the powered electrode surface, where the substrate is normally placed. Unfortunately this is a difficult experiment to perform, due to the large, time-dependent voltages on the electrode. Simulations are an ideal method of determining the dependence of parameters, such as the ion EDF, on a variety of externally determined variables, including the applied voltage, area ratio, source frequency, and background gas pressure.